Long-range transport of polluted Asian summer monsoon air to high latitudes during the PHILEAS campaign in the boreal summer 2023

M. Riese,[a,h] P. Hoor,[b] C. Rolf,[a] D. Kunkel,[b] B. Vogel,[a] F. Köllner,[b,c] M. Pöhlker,[f] F. Ploeger,[a,h] J. Ungermann,[a] W.Woiwode,[e] S. Johansson,[e] R. Bauer,[a] K. Barmpounis,[c] S. Borrmann,[b,c] P. Brauner,[c] J. Clemens,[a] A. Dragoneas,[c] F. Ekinci,[c] N. Emig,[b] A. Engel,[d] O. Eppers,[c] S. Fadnavis,[k] F. Friedl-Vallon,[e] M. Geldenhuys,[j,l] G. Günther,[a] J.U. Grooß,[a] M.I. Hegglin,[a,h] M. Höpfner,[e] M. Jesswein,[d] P. Joppe,[b,c] J. Kaumanns,[a] O. Kachula,[a] T. Keber,[d] E. Kretschmer,[e] H. C. Lachnitt,[b] V. Lauther,[h] P.E. Lloyd[f], S. Molleker,[c] R. Müller,[a] T. Neubert,[i] L. Ort,[c] U. Pöschl,[c] C. Pöhlker,[c], M. Rapp,[g] M. Retzlaff,[a] S. Rhode,[a] J. Schneider,[c] T. Schuck,[d] B.-M. Sinnhuber,[e] N. Spelten,[a] J. Strobel,[h] L. Tomsche,[b,g] K. Turhal,[h] R. van Luijt,[h] S. Versick,[e] C. Voigt,[b,g] M. Volk,[h] M. von Hobe,[a] F. Weyland,[b] A. Zahn,[e] H. Ziereis,[g] and L.O. Zlotos,[h]

[a] *Forschungszentrum Jülich GmbH (ICE-4), Jülich, Germany*

[b] *Johannes-Gutenberg University, Mainz, Germany*

[c] *Max-Planck-Institute for Chemistry Mainz. Mainz, Germany*

[d] *Goethe-University Frankfurt, Frankfurt, Germany*

[e] *Karlsruhe Institute of Technology (KIT IMKASF), Karlsruhe, Germany*

[f] *Leibniz Institute for Tropospheric Research (TROPOS), Leipzig, Germany*

[g] *Deutsches Zentrum für Luft- und Raumfahrt, Oberpfaffenhofen, Germany*

[h] *Institute for Atmospheric and Environmental Research, University of Wuppertal, Wuppertal, Germany*

[i] *Forschungszentrum Jülich GmbH (ITE), Jülich, Germany*

[j] *South African Weather Service, Gqeberha forecasting office, Gqeberha, South Africa*

[k] *Indian Institute of Tropical Meteorology, Centre for Climate Change Research, MoES, Pune, Indial*

[l] *Institute for Coastal and Marine Research, Nelson Mandela University, Gqeberha, 6001*

Corresponding author: Martin Riese, m.riese@fz-juelich.de

Early Online Release: This preliminary version has been accepted for publication in *Bulletin of the American Meteorological Society*, may be fully cited, and has been assigned DOI 10.1175/BAMS-D-24-0232.1. The final typeset copyedited article will replace the EOR at the above DOI when it is published.

ABSTRACT

The Asian summer monsoon establishes a strong connection between near-surface pollution in Southeast Asia and the global atmosphere by linking local emission sources with the large-scale circulation. There is a strong impact on the extratropical lower stratosphere, which is thought to occur mainly via quasi-horizontal export of polluted and moist air from the upper-level Asian monsoon anticyclone (AMA). The recent Probing High Latitude Export of Air from the Asian Summer Monsoon (PHILEAS) campaign focused on investigating this eddy transport and the associated mixing of monsoon-influenced air into the extratropical lower stratosphere through dedicated HALO (High Altitude and Long-Range Aircraft) observations from Oberpfaffenhofen, Germany, and Anchorage, Alaska, in the late summer and early autumn 2023.

We summarize the mission's motivation and objectives, place the Asian monsoon season 2023 into a climatological context, and present some representative observations. The observations during flights from Oberpfaffenhofen demonstrate the significant spatial and temporal AMA variability, which allowed HALO to investigate the displaced lower AMA boundary over the Eastern Mediterranean, Israel, and Jordan. The observations during flights from Anchorage highlight the influence of long-range transport of moist and polluted air from the region of the Asian summer monsoon on the composition of the extratropical upper troposphere and lower stratosphere (UTLS), which impacts both ozone chemistry and the climate-relevant radiation budget.

Accepted for publication in *Bulletin of the American Meteorological Society.* DOI 10.1175/BAMS-D-24-0232.1.

SIGNIFICANCE STATEMENT

This study examines the Asian summer monsoon's role in linking Southeast Asia's near-surface atmosphere to the global upper troposphere and lower stratosphere. We find that the Asian summer monsoon plays a key role in transporting moisture, aerosols, and pollutants (including very-short-lived chlorinated compounds) to high-latitude regions. This, in turn, impacts atmospheric chemistry including stratospheric ozone depletion, and alters the climate-relevant atmospheric radiation budget. Additionally, long-range transport of aerosols, such as ammonium nitrate, has the potential to influence cloud formation, further affecting climate and weather patterns.

CAPSULE (BAMS ONLY)

The PHILEAS campaign studied long-range transport of moisture and pollutants from the Asian summer monsoon region into the extratropical upper troposphere and lower stratosphere in August and September 2023.

Accepted for publication in *Bulletin of the American Meteorological Society.* DOI 10.1175/BAMS-D-24-0232.1.

1. Introduction

Composition changes and variability in the extratropical upper troposphere and lower stratosphere (UTLS) play an important role for near-surface climate and its variability (e.g., Lacis et al., 1990; Solomon et al., 2010; Riese et al., 2012) and for tropospheric weather patterns (Charlesworth et al., 2023; Ploeger et al., 2024). An important process is transport of moist and polluted air from the Asian summer monsoon region into the global UTLS (e.g., Randel et al., 2010; Vogel et al., 2015), affecting both the composition of the stratosphere via the tropical pipe and the extratropical lower stratosphere (e.g., Ploeger et al., 2017). The monsoon system provides a strong link between the near-surface pollution in Southeast Asia and the global circulation by convectively uplifting moist and polluted air into the subtropical tropopause region (e.g., Pan et al., 2016). Isentropic transport of this air towards higher latitudes shapes, for example, the annual water vapor cycle in the extratropical lower stratosphere (e.g., Randel and Jensen, 2013; Ploeger et al., 2013).

The Asian summer monsoon circulation is a dominant component of the regional climate system over South and Southeast Asia. It supplies most of the annual precipitation in these regions (Riehl, 1954). The monsoon is characterized by persistent convection and associated low-level cyclonic flow. This low-level cyclonic flow is dynamically coupled with an upper-level anticyclonic flow, known as the Asian Monsoon Anticyclone (AMA), which encompasses a large part of the Asian continent. The low-level cyclonic flow and the AMA are both maintained by intense diabatic heating over the Indian subcontinent and the Tibetan Plateau (Gill, 1980), as well as by the orographic forcing exerted by the plateau itself (Hoskins and Rodwell, 1995). The AMA extends vertically from approximately 12 to 18 km in altitude (Dunkerton 1995). It is dynamically bounded to the north by the subtropical westerly jet near 40°N and to the south by the tropical easterlies around 10°N. The AMA extends episodically as far west as the Eastern Mediterranean or as far east as the Asian Pacific coast and its edge acts, to some degree, as a transport barrier (Ploeger et al., 2015). Nevertheless, the AMA exhibits considerable variability in both strength and spatial extent on intraseasonal and interannual time scales (e.g., Garny and Randel, 2013; Vogel et al., 2015; Pan et al., 2016; Peña Ortiz et al., 2024).

The AMA confines convectively uplifted pollutants from Asia, particularly over regions like India, southern China, and Indonesia (e.g., Park et al., 2007; 2008). A comprehensive overview of the climatological seasonal evolution of chemical composition within the AMA

Accepted for publication in *Bulletin of the American Meteorological Society.* DOI 10.1175/BAMS-D-24-0232.1.

region (15° to 45°N and 100° to 130°E) is given by Santee et al., (2017). Their analysis is based on 10 years (2005 to 2014) of Aura Microwave Limb Sounder (MLS) version 4 satellite data, covering a wide range of tropospheric (e.g., H_2O, CO) and stratospheric (e.g., O_3, HNO_3) tracers. The paper also provides an overview of previous MLS-based studies on the export of AMA air to mid- and high latitudes (see references therein). Aircraft measurements in the center of the AMA during the StratoClim campaign in 2017 revealed the impact on the UTLS of massive uplift of NH_3 emissions in the northern part of the Indian subcontinent. Convective uplift of NH_3 during the monsoon season leads to a layer of solid ammonium nitrate aerosol particles (Höpfner et al., 2019; Appel et al., 2022), significantly contributing to the formation of the Asian tropopause aerosol layer (ATAL). These solid ammonium nitrate particles have the potential to affect cirrus cloud formation (Wagner et al., 2020).

The AMA plays an important role for the transport of tropospheric air masses into the tropical pipe, and ultimately into the deep stratosphere (e.g., Ploeger et al., 2017; Vogel et al., 2019, Yan et al., 2019). A second important transport pathway concerns the quasi-horizontal isentropic eddy transport of AMA air into the extratropical lower stratosphere at altitudes around 380 K (e.g., Gettelman et al., 2011; Ploeger et al., 2013; Müller et al., 2016; Vogel et al., 2016; Köllner et al., submitted). Eastward eddy transport is facilitated by Rossby wave breaking and the associated transport of filaments or shed eddies along the jet stream over the Pacific (e.g., Dethof et al., 1999; Hsu and Plumb, 2000; Popovic and Plumb, 2001; Vogel et al., 2014; Ungermann et al., 2016; Siu and Bowman, 2020). This transport peaks during the boreal summer months (e.g., Clemens et al., 2022). A schematic of this pathway is shown in Figure 1. Aircraft observations of anomalies of pollutants such as dichloromethane (e.g., Lauther et al., 2022) and greenhouse gases such as methane over the North Atlantic Ocean underline this significance of this transport path for the composition of the extratropical lower stratosphere during summer and early autumn. The influence is also clearly visible in the background concentrations of radiatively active species such as water vapor, methane and nitrous oxide (Müller et al., 2016; Vogel et al., 2016, 2016; Rolf et al., 2018).

The continental part of the Asian monsoon system consists of two distinct components: the South Asian summer monsoon and the East Asian summer monsoon (e.g., Pan et al., 2024), which both influence the AMA composition. While previous aircraft campaigns focused on the subtropical upper troposphere in the regions of the South Asian summer monsoon (Lelieveld et al., 2018; Tomsche et al., 2019: Höpfner et al., 2019; Adcock et al., 2021, Vogel et al., 2023)

Accepted for publication in *Bulletin of the American Meteorological Society.* DOI 10.1175/BAMS-D-24-0232.1.

or East Asian summer monsoon (Pan et al. 2024), the recent HALO campaign PHILEAS (Probing high latitude export of air from the Asian summer monsoon) provided the first in-situ observations in the Eastern Pacific region, where mixing of AMA-influenced air into the extratropical lower stratosphere occurs (e.g., Vogel et al., 2016). The campaign took place in August and September 2023 and focused on the following three scientific questions:

1) How do gas-phase and particulate constituents evolve in large-scale filaments or shed eddies originating from the AMA?
2) What are the main transport pathways and time scales of polluted and moist air from the Asian monsoon region into the extratropical UTLS?
3) What is the large-scale impact of the AMA on the background state of the extratropical lower stratosphere?

In addition, the devastating forest fires in Canada in August and September 2023 motivated some dedicated observations of associated pollutants in the second half of the campaign (see Table 1). A presentation of these observations is beyond the scope of this paper, which focusses on the main campaign objectives.

Section 2 outlines the PHILEAS campaign and HALO's capabilities. Section 3 places observations in a climatological context. Section 4 focusses on export of Asian monsoon air into the extra-topics. Section 5 assesses the main transport pathways and quantifies AMA's impact on the stratospheric water vapor budget. Finally, Section 6 summarizes some initial results and their implications.

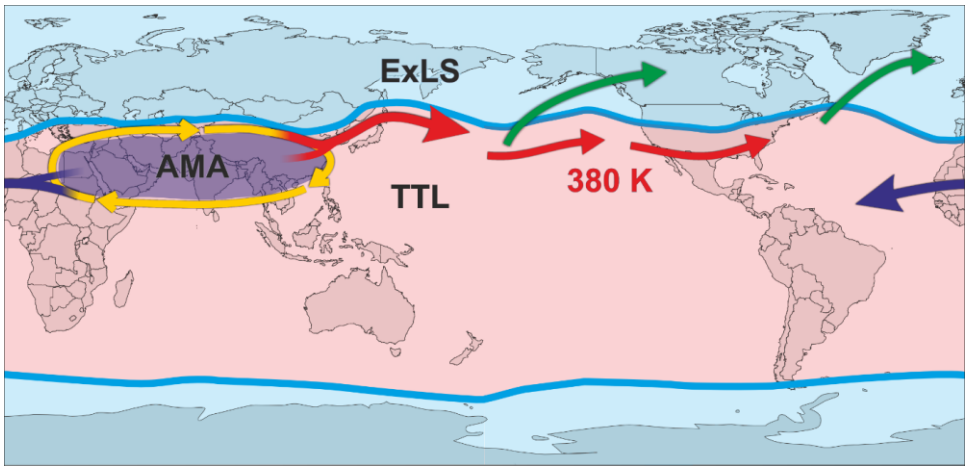

Fig.1. Schematic of the quasi-horizontal, isentropic outflow of AMA air at 380 K, adapted from Vogel et al. (2016). Yellow arrows indicate the edge of the AMA and the corresponding wind direction. Eastward and westward outflows are represented by red and blue arrows, respectively. Green arrows depict the mixing of air into the extratropical lowermost stratosphere, which was one of the main objectives of the research flights from Anchorage.

Accepted for publication in *Bulletin of the American Meteorological Society*. DOI 10.1175/BAMS-D-24-0232.1.

2. The PHILEAS aircraft campaign

The PHILEAS campaign was structured into three distinct phases to achieve its objectives. Phase 1, from 5 to 20 August 2023, focused on investigating air from the westward-displaced AMA. Phase 1 flights were conducted from Oberpfaffenhofen, Germany, towards the Eastern Mediterranean region (Figure 2, top panel). A secondary goal of Phase 1 was to probe the background state of the extratropical lower stratosphere in mid-August. This was achieved through dedicated flights towards Scandinavia, i.e. high northern latitudes. Phase 2, from 21 August to 19 September 2023, aimed at studying the transport of moist and polluted air masses across the Pacific and their mixing into the extratropical lower stratosphere. Phase 2 flights were conducted from the campaign base in Anchorage, Alaska (Figure 2, bottom panel). The final Phase 3 covered the transfer of HALO from Anchorage back to Oberpfaffenhofen and a single concluding background flight over Northern Europe. Table 1 summarizes all twenty PHILEAS flights and their primary objectives.

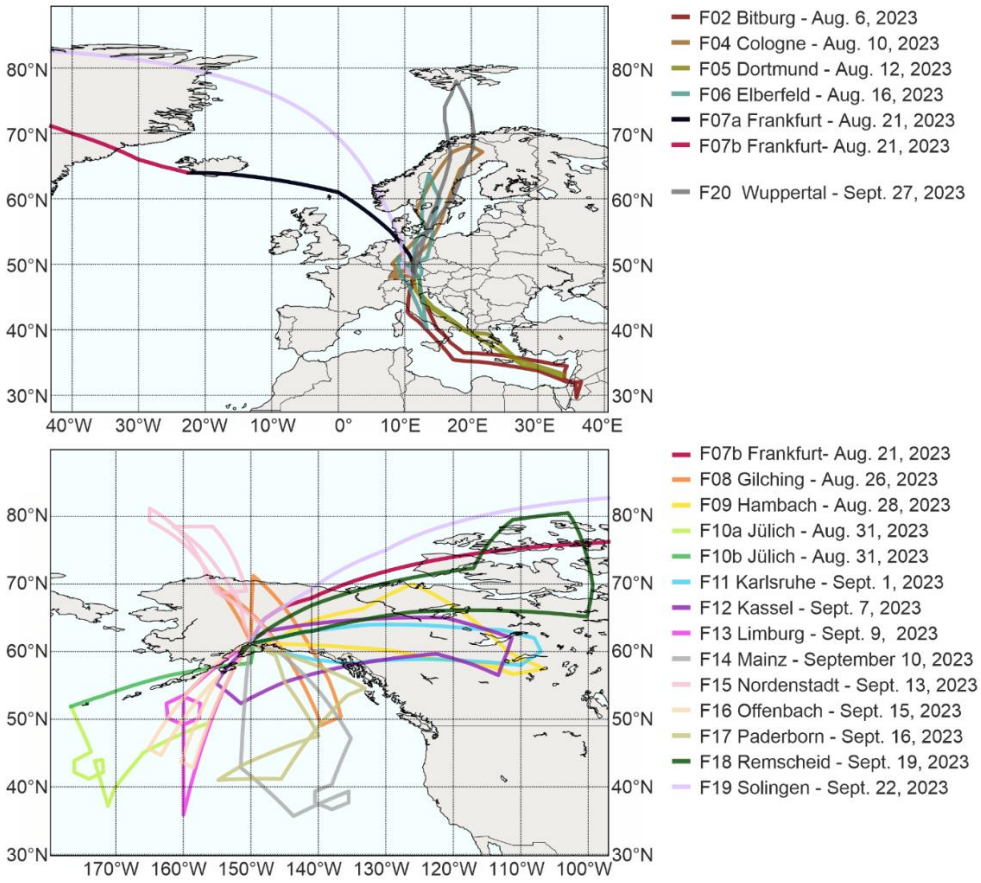

Fig. 2. (Top) HALO flight tracks during PHILEAS Phases 1 and 3 from Oberpfaffenhofen (Germany), including transfer flights. (Bottom) HALO flight tracks during PHILEAS Phase 2 from Anchorage. Each flight is labeled with a number and a city name for identification. The tracks of the electromagnetic compatibility (EMC) flight (F01) and the turbulence calibration flight (F03) are not shown.

Accepted for publication in *Bulletin of the American Meteorological Society.* DOI 10.1175/BAMS-D-24-0232.1.

The PHILEAS aircraft observations were augmented by balloon-borne measurements conducted in Nainital, India (9°23'N, 79°27'E, 1938 m above sea level). These measurements were similar in scope to those carried out during a previous campaign in Nainital in the summer of 2016 (e.g., Brunamonti et al., 2018; Hanumanthu et al., 2020; Fadnavis et al., 2023; Clemens et al., 2024). Between 14 August and 23 September 2023, a total of 16 small balloons were launched. The payloads included radiosondes, Electrochemical Concentration Cell (ECC) ozone sondes (e.g., Fadnavis et al., 2023), Cryogenic Frost Point Hygrometer (CFH) sondes (e.g., Vömel et al., 2016), and Compact Optical Backscatter Aerosol Detector (COBALD) sondes (e.g., Brabec et al., 2012). Specifically, three ozone sondes, five CFH sondes, and five COBALD instruments were deployed during the campaign.

Table 1. Overview of PHILEAS flights

Flight No.	**Date (LT)**	**Main Objectives**	**Target region**	**Operational data**
F01 "Alzenau"	27 July 2023	EMC flight	Germany	Base: Oberpfaffenhofen (EDMO) Take-Off: 0916 UTC Duration: 3.5h Flight Levels (FLs): 150, 310
F02 "Bitburg"	6 August 2023	Probe westward ASM outflow.	Eastern Mediterranean., Israel, Jordan	Base: EDMO Take-Off: 0704 UTC Duration: 9h Max. FL 470
F03 "Bahamas"	9 August 2023	Turbulence calibration	Germany	Base: EDMO Take-Off: 0910 UTC Duration: 1.5 h
F04 "Cologne"	10 August 2023	Probe old background air with little ASM influence	Sweden	Base: EDMO Take-Off: 0936 UTC Duration: 8h Max. FL 470
F05 "Dortmund"	12 August 2023	Probe westward ASM outflow	Eastern Mediterranean	Base: EDMO Take-Off: 0705 UTC Duration: 8h Max. FL 470
F06 "Elberfeld"	16 August 2023	Probe old background air with little ASM influence; Probe subtropical air masses over Italy	Sweden, Germany, Italy	Base: EDMO Take-Off: 0856 UTC Duration: 8h Max. FL 470
F07 "Frankfurt"	21 August 2023	Transfer flight to Anchorage with stop in Island	Northern Hemisphere, Alaska	Base: EDMO Take-Off: 0841 UTC Dur.: 12h (with stop) Max. FL 430
F08 "Gilching"	26 August 2023	Probe filaments with large ASM fraction; Detect in-mixing into the lower stratosphere	Alaska, Pacific Ocean	Base: Anchorage (PANC) Take-Off: 1758 UTC Duration: 8h Max. FL 470

Accepted for publication in *Bulletin of the American Meteorological Society.* DOI 10.1175/BAMS-D-24-0232.1.

F09 “Hambach”	28 August 2023	Measure above extreme wildfires in Canada; Revisit air mass with large ASM fraction (F08)	Alaska, Canada	Base: PANC Take-Off: 1819 UTC Duration: 9h Max. FL 470
F10 “Jülich”	31 August 2023	Double flight; Probe air mass with large ASM fraction over the Pacific Ocean; Probe transition from ASM air to background (hexagon)	Pacific Ocean, Adak Island	Base 1: PANC Take-Off: 1607 UTC Duration: 7h Base 2: Adak Island Take-Off: 0110 UTC Duration: 3h Max. FL 450
F11 “Karlsruhe”	1 September 2023	Resample air masses from tomographic hexagon (F10)	Alaska, Canada	Base: PANC Take-Off: 2117 UTC Duration: 6h 30min Max. FL 450
F12 “Kassel”	7 September 2023	Sample stratospheric background; Probe aged wildfire plumes	Alaska, Canada	Base: PANC Take-Off: 1805 UTC Duration: 8h Max. FL 470
F13 “Limburg”	9 September 2023	Sample two distinguished air masses with high ASM fraction; Probe transition from ASM air to background (hexagon)	Pacific Ocean	Base: PANC Take-Off: 1803 UTC Duration: 9h Max. FL 450
F14 “Mainz”	10 September 2023	Revisit distinguished air masses with a large ASM contribution (F13)	Pacific Ocean	Base: PANC Take-Off: 1959 UTC Duration: 9h Max. FL 450
F15 “Nordenstadt”	13 September 2023	Revisit distinguished air mass with large ASM fraction (F13, F14) after in-mixing into lower stratosphere	Arctic Ocean	Base: PANC Take-Off: 1802 UTC Duration: 9h Max. FL 470
F16 “Offenbach”	15 September 2023	Sample slanted filament of Asian monsoon air over the Pacific at different altitudes; Probe shear zones in the vicinity of the jet	Pacific Ocean	Base: PANC Take-Off: 2206 UTC Duration: 9h Max. FL 470
F17 “Paderborn”	16 September 2023	Follow-up of F16, Track monsoon filaments from previous day	Pacific Ocean	Base: PANC Take-Off: 2200 UTC Duration: 8.5h Max. FL 450
F18 “Remscheid”	19 September 2023	Sample background air; Resample air encountered during F17	Alaska, Canada	Base: PANC Take-Off: 2200 UTC Duration: 8.5h Max. FL 470
F19 “Solingen”	22 September 2023	Transfer flight	Northern Hemisphere, Germany	Base: PANC Take-Off: 2156 UTC Duration: 8.5h Max. FL 470
F20 “Wuppertal”	27 September 2023	Probe lower stratospheric background at the end of the monsoon season	Sweden, Svalbard	Base: EDMO Take-Off: 0738 UTC Duration: 9h Max. FL 470

Accepted for publication in *Bulletin of the American Meteorological Society.* DOI 10.1175/BAMS-D-24-0232.1.

Flight planning

All aircraft flights were planned using forecast data for chemical species and auxiliary parameters provided by the Mission Support System (MSS) (Rautenhaus et al., 2012; Bauer et al., 2022). These forecasts were generated from simulations using the Chemical Lagrangian Model of the Stratosphere (CLaMS, e.g., Pommrich et al., 2014) and the ICOsahedral Nonhydrostatic (ICON) model (Zängl et al., 2015) with the Aerosol and Reactive Trace gases (ART) module activated (e.g., Weimar et al., 2017; Schröter et al., 2018). The CLaMS model was driven by meteorological forecast data from the European Centre for Medium-range Weather Forecasts (ECMWF), while ICON-ART forecasts were initialized by meteorological analyses from the German Weather Service (DWD). Auxiliary mission planning parameters obtained from the simulations included surface-origin tracers (see also Section 3) as well as age-of-air tracers provided by CLaMS (Ploeger and Birner, 2016). The MSS planning tool facilitated mission planning by visualizing the forecasted parameters through horizontal and vertical cross sections along proposed flight tracks.

Platform and instruments

As the PHILEAS campaign focuses primarily on the extratropical UTLS, the high-flying, long-range research aircraft HALO represented an ideal mission platform (Figure 3). Equipped with an advanced payload, HALO reached altitudes up to 15 km and provided an operational range of approximately 9000 km. These capabilities enabled detailed investigations of fine-scale vertical and horizontal structures in temperature and trace gas distributions such as monsoon-influenced filaments in the extratropical UTLS, a key objective of the PHILEAS mission.

To meet the mission objectives outlined in Section 1, the observational dataset included key meteorological variables, such as temperature, and chemical tracers used to differentiate between tropospheric and stratospheric air masses. Tropospheric tracers, including water vapor and carbon monoxide (CO), originate primarily from surface sources and exhibit high mixing ratios in the troposphere that decrease sharply across the tropopause. In contrast, stratospheric tracers such as ozone and nitric acid (HNO_3) are predominantly produced in the stratosphere and exhibit strongly decreased mixing ratios in the troposphere. To identify air masses influenced by the Asian monsoon, additional tracers with tropospheric sources in the monsoon region such as dichloromethane (CH_2Cl_2) were measured. This was complemented by measurements of particle size distributions and chemical composition of aerosols.

Accepted for publication in *Bulletin of the American Meteorological Society.* DOI 10.1175/BAMS-D-24-0232.1.

Additionally, measurements of chemical species with varying lifetimes were necessary to elucidate transport pathways (and their timescales) out of the AMA. These observations were facilitated by a combination of in-situ and remote-sensing instruments, as shown in Figure 3 and listed in Table 2.

A novel aspect of PHILEAS compared to previous HALO UTLS missions (e.g. Kunkel et al., 2019, Oelhaf et al., 2019, Voigt et al., 2017) was the focus on aerosol particles, particularly solid ammonium nitrate, alongside their precursor gases (e.g., NH_3) and associated microphysical properties. To address these objectives, the payload was enhanced by the ERICA (ERC Instrument for the Chemical composition of Aerosols) aerosol mass spectrometer (Hünig et al., 2022; Dragoneas et al., 2022) and the Fast Aerosol Size Distribution (FASD) instrument (e.g., Curtius et al., 2024), designed to provide aerosol physicochemical characteristics.

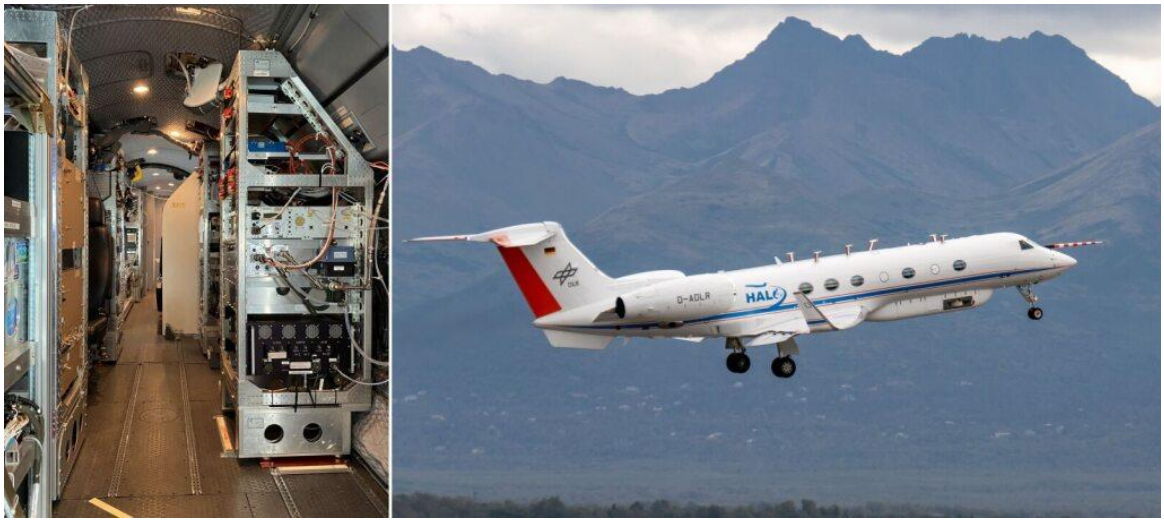

Fig.3. (Right) Takeoff of the research aircraft HALO in Anchorage. The belly pod under the front part of the fuselage houses the GLORIA infrared remote sensing instrument. The inlets on top of the fuselage provide surrounding air to the instruments inside the aircraft. (Left) View inside the HALO cabin, showing the innovative payload that combines remote sensing and in-situ instruments. Figure panels courtesy of Martin Riese (Forschungszentrum Jülich, left) and Andreas Minikin (DLR, right).

The Gimballed Limb Observer for Radiance Imaging of the Atmosphere (GLORIA) instrument (Riese et al., 2014; Friedl-Vallon et al., 2014) offered advanced two- and three-dimensional measurement capabilities, making it particularly well-suited for studying dynamical processes and trace gas structures associated with stratosphere-troposphere exchange. As part of the PHILEAS data analysis, dichloromethane (CH_2Cl_2) mixing ratio values were retrieved for the first time from GLORIA observations in the UTLS region.

Accepted for publication in *Bulletin of the American Meteorological Society.* DOI 10.1175/BAMS-D-24-0232.1.

Enhanced CH_2Cl_2 values are an excellent indicator of air originating from the region of the Asian summer monsoon (see Section 4).

GLORIA was mounted in the aircraft's belly pod, located under the forward section of the fuselage, with its field of view directed to the right relative to the flight direction (Figure 3). Optimal instrument performance is achieved at high altitudes, as the limb-sounding technique is designed for the retrieval of temperature, trace gas, and aerosol profiles from the flight level down to lower altitudes (e.g., Wetzel et al., 2021; Johansson et al., 2024).

Table 2. PHILEAS instrumentation

Instrument	Target Parameter	Technique	Institution	Reference
GLORIA	Solid ammonium nitrate, NH_3, O_3, H_2O, HNO_3, PAN, C_2H_6, C_2H_2, HCOOH, CH_2Cl_2, … temperature	Imaging IR limb sounder	ICE-4, FZ Jülich; IMK-ASF, KIT	Riese et al. (2014); Friedl-Vallon et al. (2014)
AMICA	COS, CO, CO_2	OA-ICOS	ICE-4, FZ Jülich	Kloss et al. (2021); von Hobe et al. (2021)
AIMS	HCl, HNO_3, $ClONO_2$, SO_2	Mass spectrometer	DLR-IPA, University of Mainz	Jurkat et al. (2016); Marsing et al. (2019); Tomsche et al. (2022)
BCPD	Cloud droplet size distribution	Back scatter with polarization detection	DLR-IPA	Lucke et al. (2023); Moser et al. (2023)
BAHAMAS	Meteorological and avionic data	Basic measurement and sensor system	DLR-FX	Krautstrunk and Giez (2012)
FAIRO	O_3	Chemiluminescence	IMK-ASF, KIT	Zahn et al. (2012)
FASD	Aerosol size distribution and number concentration	CPC Batterie; UHSAS	TROPOS /MPIC Mainz	Curtius et al., (2024)
FISH	Total and gas-phase H_2O	Lyman-alpha hygrometer	ICE-4, FZ-Jülich	Zöger et al. (1999); Meyer et al. (2015)
GhOST-MS	SF_6, CFCs, CH_3Br, $CHBr_3$, $CHCl_3$, …	Gas chromatograph – Mass spectrometer	University of Frankfurt	Keber et al. (2020)
HAGAR-V	CO_2, SF_6, CFCs, HCFCs, HFCs, halogenated VOCs, NMHCs	NDIR; GC-ECD; GC-MS	University of Wuppertal	Lauther et al. (2022)
AENEAS	NO, NO_y	Chemiluminescence	DLR-IPA	Ziereis et al. (2022)
ERICA	Aerosol composition and size distribution (d >120nm)	Mass spectrometer	University of Mainz; MPIC Mainz	Hünig et al. (2022); Dragoneas et al. (2022)
UMAQS	CO, N_2O, CH_4, C_2H_6	QCL absorption spectrometer	University of Mainz	Müller et al. (2015); Kunkel et al., (2019)

Accepted for publication in *Bulletin of the American Meteorological Society.* DOI 10.1175/BAMS-D-24-0232.1.

The instrument's high measurement speed enabled dense sampling along the flight path, resulting in two-dimensional curtains of trace gas distributions with a horizontal sampling of approximately 3.5 km. For three-dimensional tomographic measurements, hexagonal flight patterns were employed (e.g., Ungermann et al., 2011; Kaufmann et al., 2015; Krasauskas et al., 2021), resulting in a horizontal resolution of up to 20 km × 20 km and a vertical resolution of approximately 300 m.

3. PHILEAS in a climatological context

To classify PHILEAS observations within a climatological context, atmospheric transport from the Asian summer monsoon region in September 2023 is compared to a 23-year September climatology spanning 2000–2022. This analysis employs surface-origin tracers (e.g., Vogel et al., 2015, 2016) integrated into the transport models of CLaMS and ICON-ART (Figure 4). The tracers are used to identify air masses uplifted by the Asian summer monsoon and subsequently transported to higher latitudes. The CLaMS simulations are initialized annually on May 1st, covering the period from the pre-monsoon to the post-monsoon seasons. The simulations are driven by horizontal winds derived from the ERA5 reanalysis dataset provided by ECMWF (Hersbach et al., 2020), downscaled to a horizontal resolution of 1° × 1° (e.g., Ploeger et al., 2021; Clemens et al., 2024). Surface-origin tracers are released every 24 hours within the boundary layer, approximately 2–3 km above the surface in the specific regions shown in Figure 4. These tracers are subsequently transported (advected and mixed) into the free atmosphere over the course of the simulation, from May 1 to October 31.

To specifically track Asian monsoon air masses, a marker termed the "South Asia tracer" is defined, encompassing the continental regions as well as parts of the Indian Ocean and the Bay of Bengal (Figure 4). The inclusion of the Indian Ocean accounts for clean, moist air masses originating in the Indian Ocean boundary layer that are transported northward over the Indian subcontinent. During this transport, these air masses can take up heavily polluted air from the Indo-Gangetic Plain, a densely populated and industrialized region, before being uplifted into the UTLS (e.g., Fadnavis et al., 2013; Lau et al., 2018; Vogel et al., 2023). In addition, a Western Pacific surface-origin tracer is used in the forecast system, which predominantly represents maritime-influenced regions such as the Western Pacific, Southeast Asia, and the warm pool (e.g., Vogel et al., 2016).

Accepted for publication in *Bulletin of the American Meteorological Society.* DOI 10.1175/BAMS-D-24-0232.1.

The AMA composition is strongly influenced by the intensity of convective uplift associated with the South Asian and East Asian summer monsoons. Pan et al. (2024) reported a stronger-than-average East Asian summer monsoon during the Asian Summer Monsoon Chemical & Climate Impact Project (ACCLIP) campaign in 2022, based on CO data (147 hPa) obtained from Microwave Limb Sounder (MLS) observations (Waters et al., 2006).

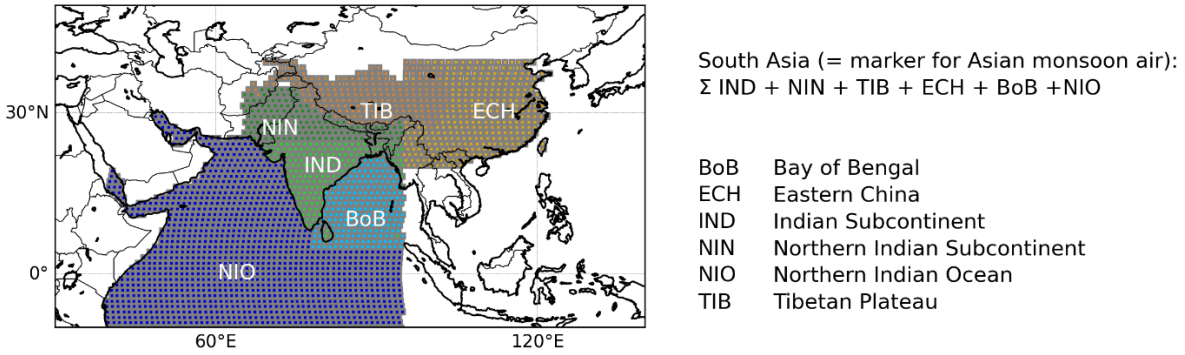

Fig. 4. Surface-origin tracers used to forecast air masses convectively lifted by the Asian Summer Monsoon. CLaMS simulations begin on May 1st and cover the pre-monsoon to post-monsoon period. Surface-origin tracers are released every 24 hours within the boundary layers of the defined model regions, as indicated by the shaded areas. The ‘‘South Asia tracer’’ encompasses all these regions and served as a key component in the PHILEAS flight planning.

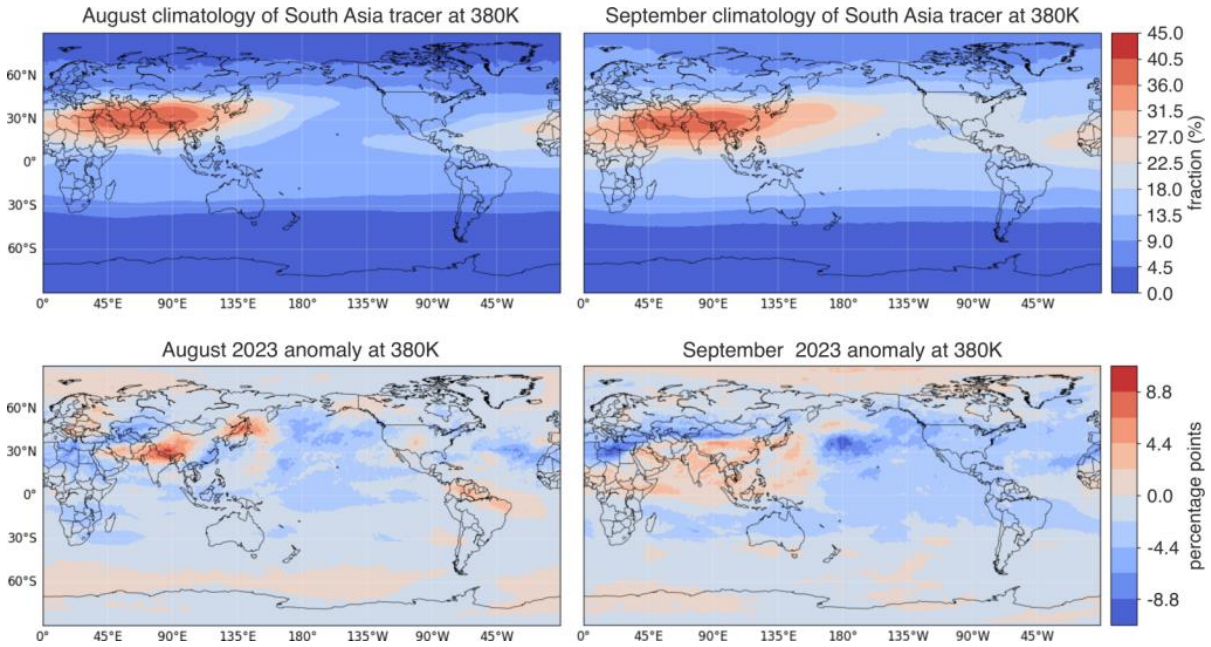

Fig. 5. (Top) 23-year climatology (2000 to 2022) of the South Asia surface-origin tracer at 380 K for August (left) and September (right). Prominent features are the AMA and the trace of eastward eddy transport. (Bottom) Residual difference between the South Asia surface-origin tracer percentage contribution in August 2023 (left) and September 2023 (right) and the 23-year September climatology. The residual indicates a stronger-than-average flushing of the deeper extratropical lower stratosphere in September 2023.

Accepted for publication in *Bulletin of the American Meteorological Society.* DOI 10.1175/BAMS-D-24-0232.1.

The climatological AMA signature at 380 K (see also Santee et al., 2017) and the path of the eastward eddy transport are shown in Figure 5 (top) for August and September based on the 23-year average of the tracer originating from South Asia (South Asia surface-origin tracer). During the PHILEAS period, the tracer anomaly at 380 K (Figure 5, bottom) shows slightly elevated values in the center of the South Asian summer monsoon and downstream of the East Asian summer monsoon. However, the latter is less pronounced than in the 2022 ACCLIP season, as indicated by the CLaMS simulations of a uniformly emitted tracer (E90) with a lifetime of 90 days (not shown). Furthermore, the South Asia surface-origin tracer anomalies indicate an above-average flushing of the extratropical lowermost stratosphere.

4. Probing westward AMA extent and eastward outflow

Westward AMA extent

The AMA exhibits substantial variability in its spatial extent (e.g., Garny and Randel, 2013). Consequently, it was initially uncertain whether the AMA and the associated Asian Tropopause Aerosol Layer (ATAL) could be effectively sampled within a single research flight from the campaign base in Germany. However, a particularly favorable meteorological situation emerged before the first research flight (F02) on 6 August.

Figure 6 illustrates the large-scale distribution of the South Asia surface-origin tracer at the 360 K isentropic level (color shading) at 1200 UTC on 6 August 2023. Under these conditions, the AMA's influence extended prominently into the eastern Mediterranean region. The flight path of HALO (depicted by the white line) reveals that approximately half of the measurements were conducted in stratospheric air masses (western segment), while the other half occurred in upper tropospheric air influenced significantly by the AMA (eastern segment). Figure 6b provides a zoomed-in view of the HALO flight path, with the flight direction indicated by white arrows. Flight F02 lasted approximately 9 hours, beginning with the takeoff at 0704 UTC. To align the asynoptic measurement locations with the synoptic model output, the actual flight positions were extrapolated to 1200 UTC positions using forward and backward trajectories. These extrapolated positions are shown in Figure 6 as gray and black lines. The gray segment represents the extrapolation of the 1115 to 1515 UTC segment of the return leg. Figure 7 shows the corresponding remote sensing and in-situ measurements.

Figure 7 a and b show 2D distributions of solid ammonium nitrate concentrations and ozone mixing ratios derived from GLORIA infrared limb measurements along the flight path. For

Accepted for publication in *Bulletin of the American Meteorological Society.* DOI 10.1175/BAMS-D-24-0232.1.

orientation purposes, the 350 K, 370 K, 390 K isolines and the 2 PVU contour are superimposed on the 2D distributions. GLORIA's field of view is directed to the right with respect to the flight direction (Figure 3). The vertical measurement range shown in Figure 7 extends from the flight altitude at about 14.5 km down to 8 km. The limb geometry results in a horizontal averaging of atmospheric constituents of about 50 to 100 km at flight altitude. GLORIA remote sensing data are supplemented at the flight altitude by in-situ measurements of dichloromethane (CH_2Cl_2) mixing ratio values from HAGAR (Fig. 7c), aerosol composition data from ERICA (Fig. 7d) and aerosol size distribution data from FASD (Fig. 7e).

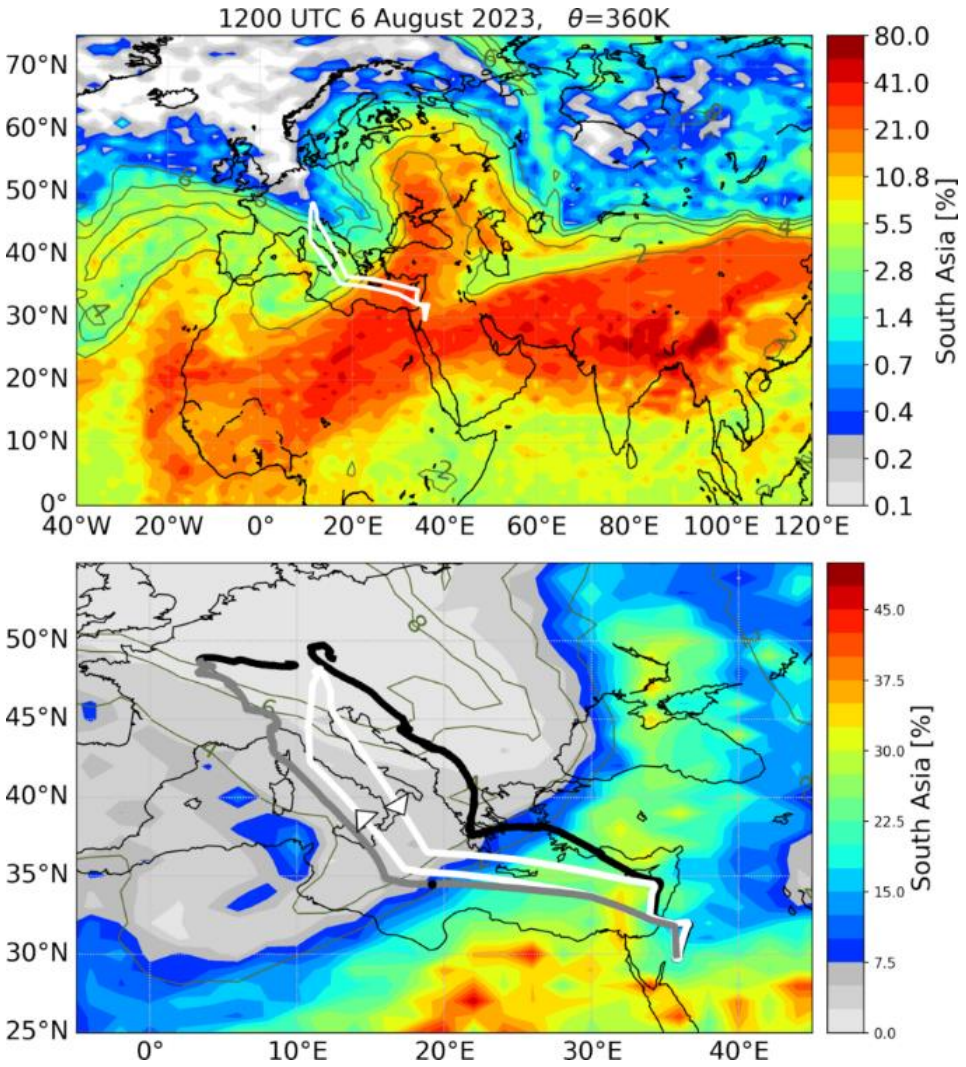

Fig. 6. Westward extent of the AMA on 6 August 2023 at 360 K. The figure shows the percentage contribution of the South Asia surface-origin tracer at 360 K (12:00 UTC) based on a CLaMS simulation driven by ERA-5. The HALO flight track is indicated by the white line. To delineate the edge of the AMA, potential vorticity (PV) isolines (2, 4, 6, 8 PVU) are included as thin olive lines. (a, top) Large-scale situation (b, bottom) Zoom-in of the region of the flight track with the calculated synoptic flight track position at 12:00 UTC shown by the black and gray lines.

Accepted for publication in *Bulletin of the American Meteorological Society.* DOI 10.1175/BAMS-D-24-0232.1.

The spatial distribution of the South Asian surface-origin tracer depicted in Figure 6b is in impressive agreement with the in situ measurements of dichloromethane (CH_2Cl_2) shown in Figure 7c. CH_2Cl_2 is an excellent tracer for air masses originating from the Asian summer monsoon region (Lauther et al., 2022), with nearly 90% of global emissions attributed to South Asia (e.g., Claxton et al., 2020). The observed CH_2Cl_2 mixing ratio decrease from approximately 100 ppt to 40 ppt in the time span from 1300 and 1330 UTC. This indicates the transition from monsoon-influenced air to undisturbed air. For comparison, the 1330 UTC position of HALO is marked by a black dot on the synoptic flight path in Figure 6b. The change in air mass character in this region is also clearly reflected in the GLORIA ozone measurements: prior to 1330 UTC, tropospheric characteristics are prevalent above the 350 K isentrope, afterwards elevated ozone mixing ratios (~0.3 ppmv) indicate the stratospheric character of the air masses encountered by HALO.

An important question prior to Flight 02 was whether signatures of the ATAL could be detected within the outflow of the westwardly displaced AMA. Until now, such signatures had not been observed this far west. Indeed, in situ aerosol composition measurements by ERICA show elevated concentrations of nitrate at around 14 km altitude around 1130 UTC, coinciding with the region of enhanced valued of the South Asia surface-origin tracer. ERICA also shows elevated concentrations of nitrate between 1200 and 1245 UTC, which correspond closely to a localized region of significantly elevated solid ammonium nitrate concentrations observed by GLORIA at flight altitude (Figure 7a). Both data sets suggest an internal structure of the AMA-influenced air massed, possibly with varying degrees of influence from different source regions. Overall, the findings are consistent with previous ERICA and GLORIA observations of the ATAL over India, where solid ammonium nitrate and organic compounds were identified as the dominant aerosol components in the accumulation mode (e.g., Höpfner et al., 2019; Appel et al., 2022). The presence of solid ammonium nitrate (Fig. 7a) is primarily attributed to new particle formation above the monsoon convective tops, followed by gradual growth during slow vertical transport within the AMA (Weigel et al., 2021; Mahnke et al., 2021; Xenofontos et al., 2024) and horizontal redistribution towards the eastern mediterranean region. These accumulation-mode particles are effectively detected by ERICA. Particularly, a good correlation between elevated nitrate concentrations measured by ERICA and enhanced number concentrations in the accumulation mode observed by FASD is found between 1115 and 1200 UTC (see Fig. 7).

Accepted for publication in *Bulletin of the American Meteorological Society.* DOI 10.1175/BAMS-D-24-0232.1.

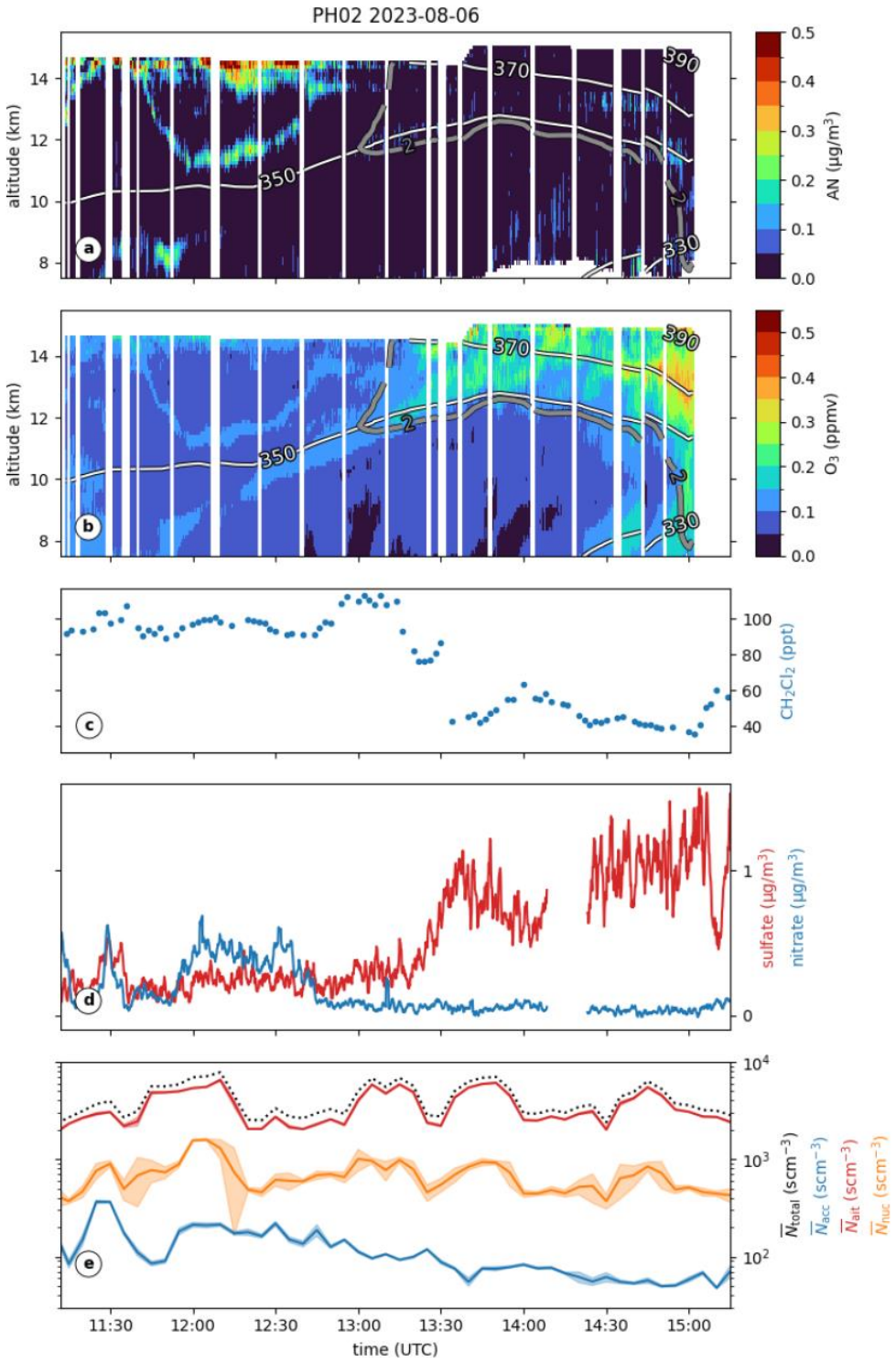

Fig. 7. Flight F02 observations on 5 August 2023 (during the return leg from Jordan to Germany). (a, b) GLORIA observations of solid ammonium nitrate and ozone. Thick gray lines represent the 2 and 6 PVU contours. The thin gray lines show the 350 K, 370 K, and 390 K isentropic levels. (c) HAGAR-V in-situ CH_2Cl_2 measurements. (d) ERICA in-situ aerosol composition measurements (1 minute means). To facilitate the comparison between AN data from GLORIA and nitrate data from ERICA, normal temperature and pressure concentrations are shown in both cases. (e) FASD aerosol number concentrations incl. standard error. Particle sizes in panel e are 2-12 nm for the nucleation mode (N_{nuc}), 12-60 nm for the Aitken mode (N_{ait}), and 60-1000 nm for the accumulation mode N_{acc}.

Accepted for publication in *Bulletin of the American Meteorological Society.* DOI 10.1175/BAMS-D-24-0232.1.

Outside of the AMA outflow (flight track from 1315 to 1515 UTC), increasing sulfate concentrations (Figure 7d) are observed alongside rising ozone mixing ratios (Figure 7b), consistent with the presence of sulfuric acid aerosol droplets from the Junge stratospheric aerosol layer (Kremser et al., 2016).

Eastward transport of filaments from the Asian summer monsoon

Phase 2 focused on investigating the eastward outflow of the AMA. In the monsoon season, eastward transport of air masses from the region of the Asian monsoon frequently occurs through the Rossby wave breaking and the associated transport of filaments along the jet stream over the Pacific (e.g. Homeyer et al., 2011, Homeyer and Bowman 2013, Vogel et al., 2016).

The objective of the first flight (F08) out of Anchorage on 26 August 2023, was to study two filamentary structures over Alaska, characterized by a large percentage of the South Asia surface-origin tracer in the forecast. The meteorological condition during is depicted in Figure 8, showing ERA5 potential vorticity data (1° x 1° horizontal resolution) over the Northern Pacific at the 380 K potential temperature level. A strong Rossby wave breaking event developed between 24 August and 27 August 2023 (Figure 8a-d). During this event, tropospheric air was deflected to the North along an Aleutian trough and a cyclonic flow developed southward, which resulted in tropospheric air masses being transported northward of stratospheric air masses. The large-scale stirring due to the breaking wave led to pronounced filamentation and subsequent mixing.

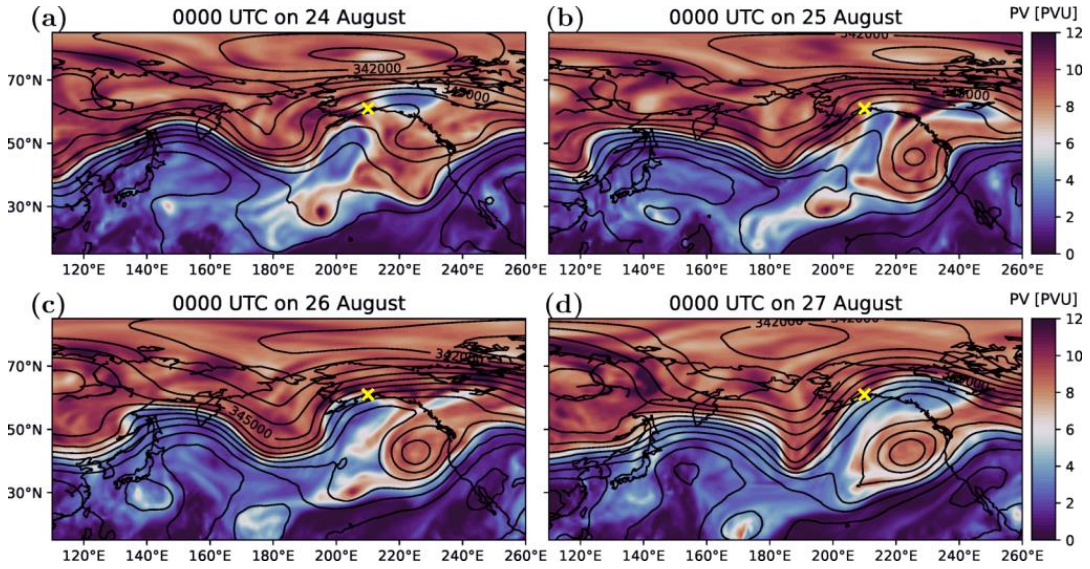

Fig. 8. Temporal evolution of ERA5 potential vorticity at 360 K over the Northern Pacific for August 24, 25, 26, and 27, 2023 (00:00 UTC). Tropospheric values are shown in blueish, and stratospheric values in redish colors. Solid black lines represent contour lines of the Montgomery stream function, the equivalent to the geopotential on isentropic surfaces. The location of Anchorage is indicated by the yellow cross.

Accepted for publication in *Bulletin of the American Meteorological Society.* DOI 10.1175/BAMS-D-24-0232.1.

Figure 9a illustrates this large-scale situation based on the South Asia surface-origin tracer at the 350 K isentropic level at 0000 UTC on 27 August 2023. Figure 9b provides a zoomed-in view of the HALO flight path, with the flight direction indicated by white arrows. The northward deflected air masses contain fine filamentary structures, which were sampled twice by HALO. After completing a southeastward leg through the filaments at altitudes between about 330 K and 350 K, HALO continued northwestward to sample the two filaments at higher altitudes between approximately 370 and 390 K. The synoptic flight path, which marks the South Asia surface-origin tracer values at the time of the actual HALO measurement (see above), is shown by the black and gray lines.

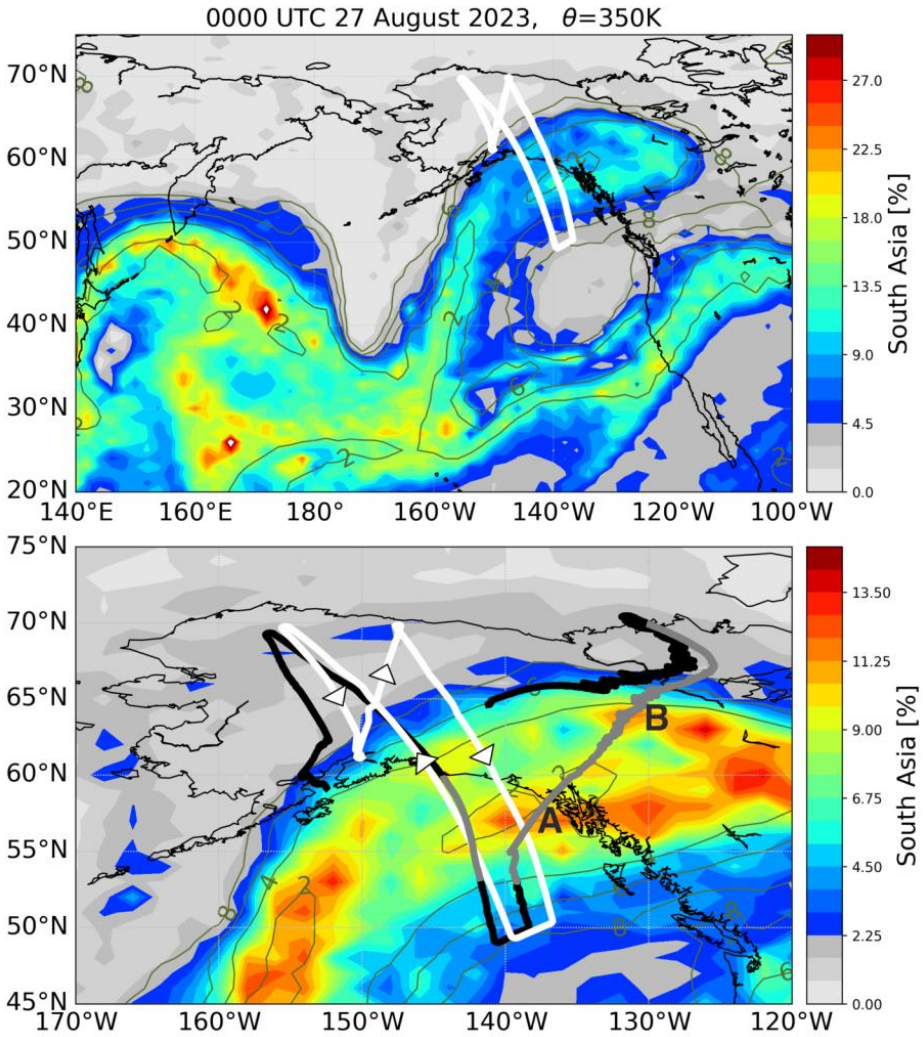

Fig. 9. South Asia surface-origin tracer at the 350K surface over the Northern Pacific on 0000 UTC on 27 August. The tracer distribution is based on a CLaMS simulation driven by ERA-5. The HALO flight track is shown by the white line. To delineate the edge of the AMA, potential vorticity (PV) isolines (2, 4, 6, 8 PVU) are included as thin olive lines. (a, top) Large-scale situation; (b, bottom) Zoom-in of the region of the flight track, with the calculated synoptic flight track position at 12:00 UTC shown by the black and gray lines. Note the different color scale used for the zoom-in. For more details see text.

Accepted for publication in *Bulletin of the American Meteorological Society.* DOI 10.1175/BAMS-D-24-0232.1.

During the southeastward leg, both the GhOST and HAGAR-V instruments consistently detected substantially enhanced CH_2Cl_2 mixing ratios, an important ozone-depleting very short-lived substance. Figure 10 shows the CH_2Cl_2 in situ measurements for the whole 8 hours flight period (takeoff 1758 UTC). The two peaks in CH_2Cl_2 mixing ratios observed between 1915 and 2130 UTC are highlighted in Figure 10 by gray shading. They exhibit mixing ratio values up to 250 ppt at around 330 K in the troposphere. The gray line in Figure 9b represents the synoptic HALO flight segment corresponding to the gray shading in Figure 10. The associated South Asia surface-origin tracer distribution also indicates the presence of two distinctive filaments. To show the good correspondence between the simulation results and the measurements better, the filaments in Figures 9 and 10 are labeled with the letters "A" and "B", respectively.

During Flight 17 (not shown), even higher CH_2Cl_2 mixing ratios of nearly 450 ppt were observed by GLORIA infrared limb observations in the upper troposphere over the Pacific. Such CH_2Cl_2 mixing ratios are close to the record values reported by Pan et al. (2024) for the ACCLIP campaign in 2022. This is notable as the PHILEAS observations, in contrast to ACCLIP measurements, were made far from the industrial source regions in Shandong and Hebei, North China (e.g., An et al., 2021). The observations therefore highlight the significant role of long-range pollutant transport in monsoon filaments. This is consistent with the findings by Lauther et al. (2022), who observed elevated CH_2Cl_2 mixing ratios even over the Atlantic Ocean during the WISE campaign in 2017 and attributed them to Asian summer monsoon air.

Figure 10 also shows the mixing ratios of chloroform ($CHCl_3$) and dibromomethane (CH_2Br_2) observed by both instruments. Notably, the CH_2Br_2 mixing ratio does not show a pronounced increase in the first filament (A) around 19:30 UTC. This suggests that the air masses in the two filaments originate from different source regions. Our findings are further evidenced by Jesswein et al. (2025), who analyze the origin of the elevated CH_2Cl_2 mixing ratios based on simulations with the Lagrangian particle dispersion model FLEXPART (Bakels et al., 2024).

The subsequent northwestward leg and the follow-on shorter southeastward leg were conducted at higher altitudes between 370 and 390 K. To better represent the meteorological conditions encountered by HALO, Figure 11 displays the South Asia surface-origin tracer distribution at the 390 K isentropic level. The gray segment of the flight track (Fig. 11b)

Accepted for publication in *Bulletin of the American Meteorological Society.* DOI 10.1175/BAMS-D-24-0232.1.

indicates the time interval from 0100 to 0145 UTC during which HALO entered stratospheric air significantly influenced by AMA.

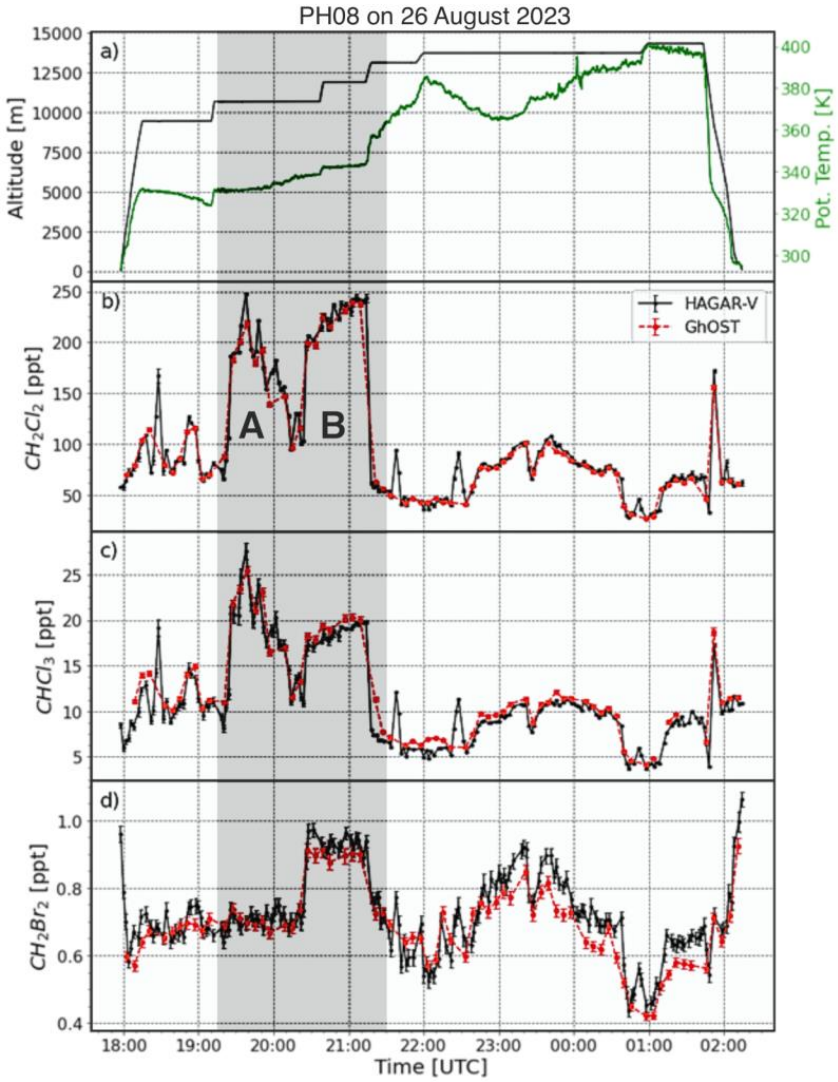

Fig. 10. Mixing ratios of CH_2Cl_2, $CHCl_3$, and CH_2Br_2 measured by the HAGAR-V and GhOST instruments during Flight 08 on 26 August 2023. The good agreement between the data of both instruments can be seen as a consistency check, underlining the high quality of the measurement data. (Top) Flight altitude (black line) and corresponding potential temperature (green line). The time interval of the gray shading corresponds to the gray part of the synoptic flight track in Figure 9b.

Figure 12 shows remote sensing and in-situ measurements acquired on these two segments from 2200 UTC on 26 August 2023 to 0145 UTC on 27 August 2023. Figures 12 a, b, and c show 2D distributions of ammonium nitrate concentrations, ozone mixing ratios, and dichloromethane mixing ratios derived from GLORIA infrared limb measurements along the flight path, respectively. The vertical measurement range extends from the flight altitude at about 14.5 km down to the altitude, where the GLORIA infrared limb observations encountered

Accepted for publication in *Bulletin of the American Meteorological Society.* DOI 10.1175/BAMS-D-24-0232.1.

clouds. As in Figure 7, the remote sensing data are supplemented at flight altitude by in-situ measurements of aerosol composition obtained from ERICA (Fig. 12d) and aerosol size distribution data from FASD (Fig. 12e).

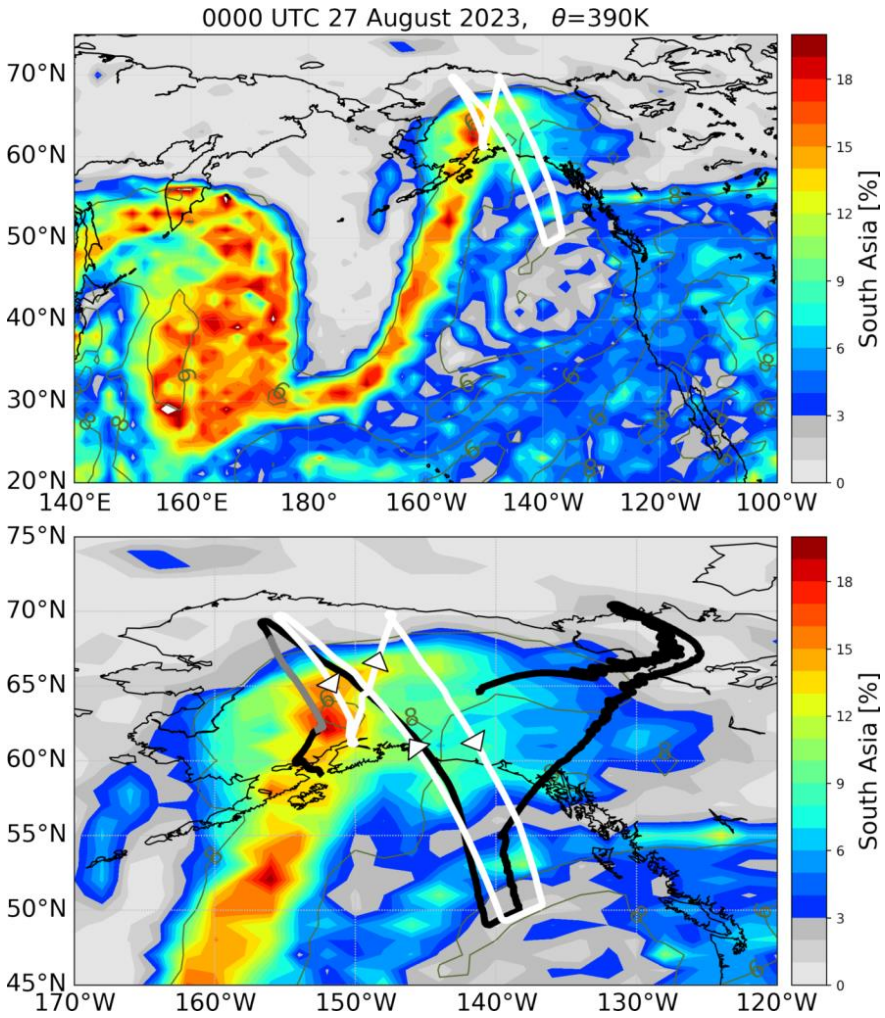

Fig. 11. South Asia surface-origin tracer at the 390K surface over the Northern Pacific on 0000 UTC on 27 August. The tracer distribution is based on a CLaMS simulation driven by ERA-5. The flight track is shown by the white line. To delineate the edge of the AMA, potential vorticity (PV) isolines (2, 4, 6, 8 PVU) are included as thin olive lines. (a, top) Large-scale situation; (b, bottom) Zoom-in of the region of the track, with the calculated synoptic flight track position at 12:00 UTC shown by the black and gray lines. For more details see text.

Between 2230 and 2315 UTC, GLORIA viewed in the direction of the air masses with enhanced CH_2Cl_2 values that had previously been probed by HAGAR-V and GhOST in-situ measurements during the southeastward leg about 3.5 hours earlier (Fig. 10). The flight path was planned so that the GLORIA tangent point locations coincided with the measurement locations of the in-situ instruments (at an altitude of approximately 11 km). Indeed, GLORIA measured significantly elevated CH_2Cl_2 concentrations between 2230 and 2315 UTC, spanning a vertical range of at least 3 km. The corresponding segment of the northwesterly flight leg is

Accepted for publication in *Bulletin of the American Meteorological Society.* DOI 10.1175/BAMS-D-24-0232.1.

indicated by the gray-shaded portion of the synoptic flight path in Figure 9. Evidently, during this time, GLORIA was observing the region of the first filament (marked by an "A" in Figs. 9 and 10). Overall, good agreement between GLORIA remote sensing observations (Fig. 12c) and the in-situ measurements is found in terms of absolute values.

During the subsequent phase of the flight from 2345 to 0030 UTC, HALO encountered regions with elevated concentrations of solid ammonium nitrate and organics at altitudes above 370 K, consistently measured by GLORIA and ERICA (compare Fig.12a with Fig. 12c).

Research aircraft such as HALO can reach their highest altitudes toward the end of a scientific flight, once a substantial portion of the fuel has been consumed. During Flight 08, HALO ascended to the 390 K isentropic level at 0100 UTC and stayed there for about 45 minutes, before the descend. The stratospheric character of the air mass is indicated by relatively high ozone levels. Interestingly, the South Asia surface-origin tracer distribution (Fig. 11b) indicates a significant AMA influence during this flight leg. Prior to the descent, obviously a mixing layer was traversed. The concurrent presence of high ozone concentrations and elevated concentration of ammonium nitrate and organic aerosol suggests an ongoing in-mixing of AMA-influenced air into the extratropical lower stratosphere. As anticipated, the elevated concentrations of ammonium nitrate and organic compounds correspond with elevated levels in the FASD aerosol number concentrations of the accumulation mode (Figure 12e). Remarkably, the nucleation mode makes a substantial contribution to the total aerosol number concentration in the mixing area, whereas the Aitken mode predominates in all other regions (see also Figure 7e).

Accepted for publication in *Bulletin of the American Meteorological Society.* DOI 10.1175/BAMS-D-24-0232.1.

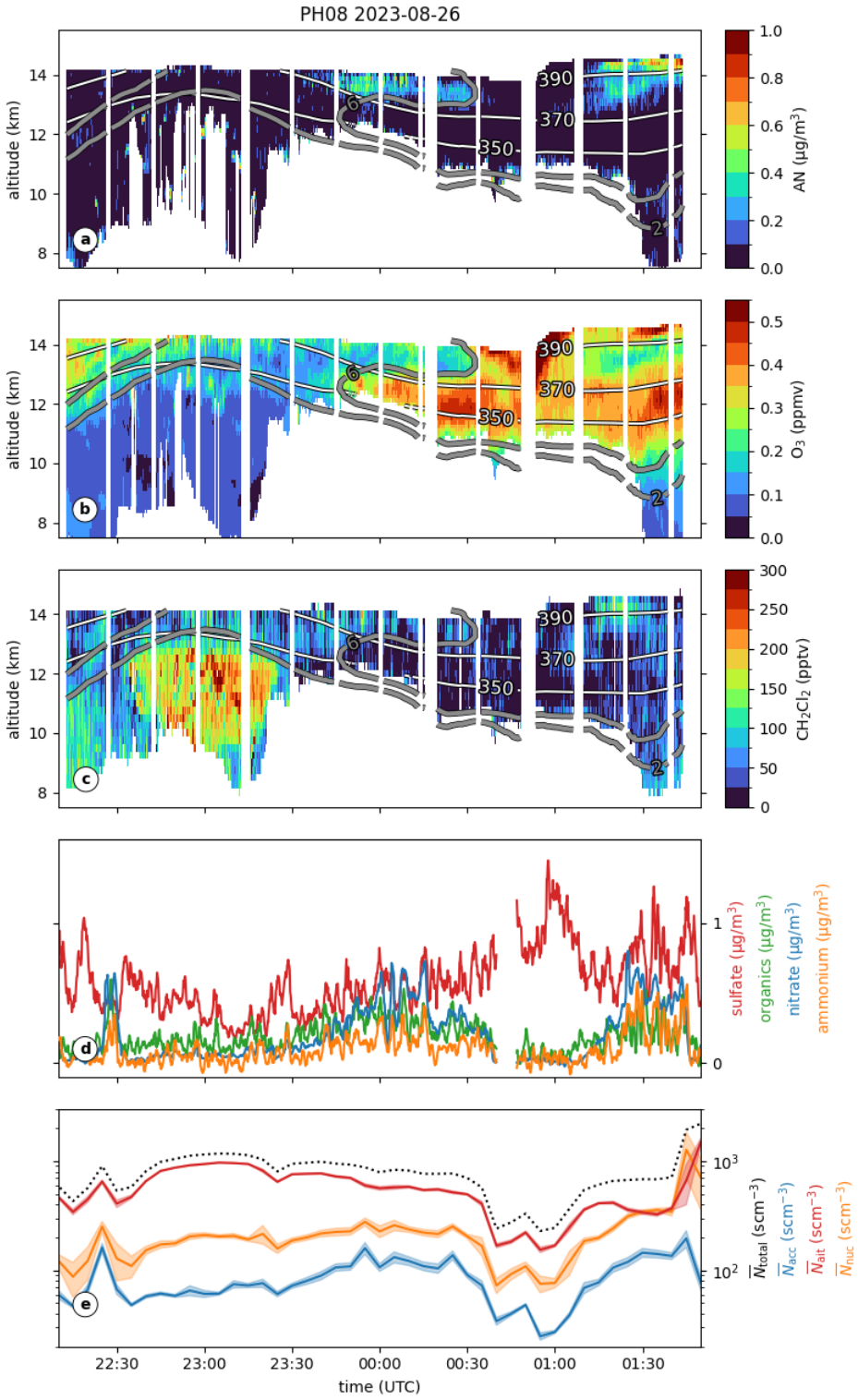

Fig. 12. HALO observations during Flight 08 on 26 August 2023. (a, b, c) GLORIA observations of solid ammonium nitrate (AN) particles, ozone, and CH_2Cl_2. Thick gray lines represent the 2 and 6 PVU contours. The thin gray lines show the 350 K, 370 K, and 390 K isentropic levels. (d) ERICA in-situ aerosol composition measurements (1 minute means). (e) FASD aerosol number concentrations incl. standard error. To facilitate the comparison between AN data from GLORIA and aerosol composition data from ERICA, normal temperature and pressure concentrations are shown in both cases. Particle sizes in panel e are 2-12 nm for the nucleation mode (N_{nuc}), 12-60 nm for the Aitken mode (N_{ait}), and 60-1000nm for the accumulation mode N_{acc}.

Accepted for publication in *Bulletin of the American Meteorological Society.* DOI 10.1175/BAMS-D-24-0232.1.

5. Impact on the extratropical lower stratosphere

Our measurements underscore the significance of different transport pathways from the Asian summer monsoon region into the extratropical lower stratosphere. The export of AMA air is mainly facilitated quasi-horizontal at high altitudes (> 370 K) in the tropopause region. This transport pathway is also essential for the distribution of aerosols into the extratropical lower stratosphere, which have been produced in the ATAL region by gas-to-particle conversion (Köllner et al., submitted). Transport at lower altitudes is evidenced by the elevated CH_2Cl_2 mixing ratios presented in Figure 10 (see also Jesswein et al., 2025).

In Section 4, we presented one representative example of eastward transport of filamentary structures from the Asian summer monsoon into the extratropical stratosphere. However, during PHILEAS, the transport of moist and polluted air masses across the Pacific and their mixing into the extratropical lower stratosphere was investigated during a total of 11 research flights from Anchorage. This extensive dataset also enables a statistical analysis based on in situ measurements. Figure 13 illustrates different pathways using methane observations obtained from UMAQS, plotted as function of nitrous oxide (N_2O) and potential temperature. N_2O values below 336 ppb are assumed to be indicative for stratospheric air. The top panel displays the mean methane values encountered during Phase 2 and the bottom panel presents the methane anomaly, i.e. the maximum methane value of each bin minus the mean value. The high methane anomaly between 380 K and 400 K indicates polluted AMA air in the lower stratosphere, while the anomalies at lower potential temperature heights point to the "tropospheric pathways" from the Asian summer monsoon region. The relative importance of these different pathways for the entry of air masses from the Asian summer monsoon into the extratropical lower stratosphere remains to be clarified.

A central question for PHILEAS is the extent to which in-mixed humid air masses from the Asian monsoon region influence average concentrations of water vapor in the lowermost stratosphere quantitatively. Previous studies (Randel and Jensen, 2013; Ploeger et al., 2013) have shown that the annual cycle of water vapor in the extratropical lower stratosphere is strongly modulated by the in-mixing of monsoon-influenced moist air masses. This is particularly important because variations in water vapor in this region have a significant impact on the Earth's radiation balance (e.g. Riese et al., 2012).

Accepted for publication in *Bulletin of the American Meteorological Society.* DOI 10.1175/BAMS-D-24-0232.1.

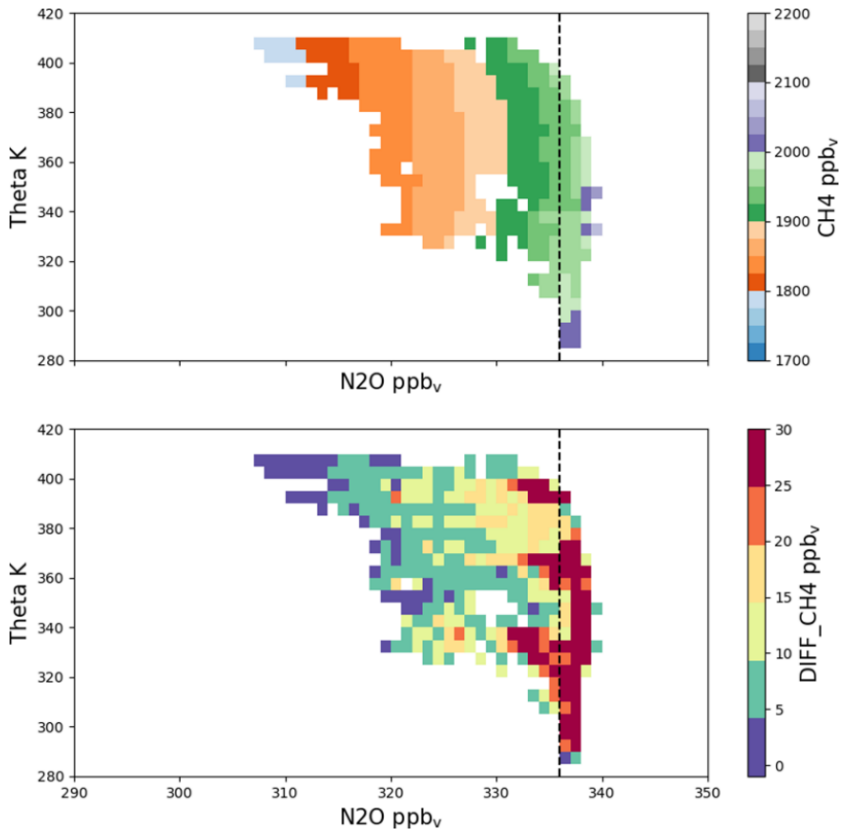

Fig. 13. Observed methane (colored shading) as a function of observed nitrous oxide (N_2O) and potential temperature. N_2O values below 336 ppb indicate stratospheric air. (Top) Mean methane values encountered in each bin during PHILEAS Phase 2. (Bottom) Methane anomaly (Maximum values in each bin minus mean values). The high methane anomalies around 340 K and 390 K suggest distinct pathways of polluted air originating from the Asian summer monsoon.

To address this question, we first compute the average water vapor profile in the lower stratosphere during the period of the PHILEAS measurements. Figure 14 presents this average profile for all observations made by the Fast In-Situ Stratospheric Hygrometer FISH (Zoeger et al., 1999) with potential vorticity (PV) values greater than 6 PVU (black line). To assess the influence of air masses originating from the Asian monsoon region, we also derive a corresponding profile, based solely on measurements with relatively low methane concentrations, i.e. a neglectable monsoon influence (blue line in Figure 14). Here, we follow the analysis by Rolf et al. (2018), who used a methane threshold of <1850 ppbv to classify air masses as not influenced by the Asian summer monsoon.

A comparison between the monsoon-affected profile (black line) and the "undisturbed" background profile (blue line) reveals an increase of approximately 0.8 ppm in water vapor within the extratropical lower stratosphere at potential temperature levels between 355 and 410 K (Figure 14, right panel). Rolf et al. (2018) found a similar water vapor increase of

Accepted for publication in *Bulletin of the American Meteorological Society*. DOI 10.1175/BAMS-D-24-0232.1.

approximately 0.5 ppm (11%) during the monsoon season 2012 from August to September in the extratropical lower stratosphere at a potential temperature level of 380 K.

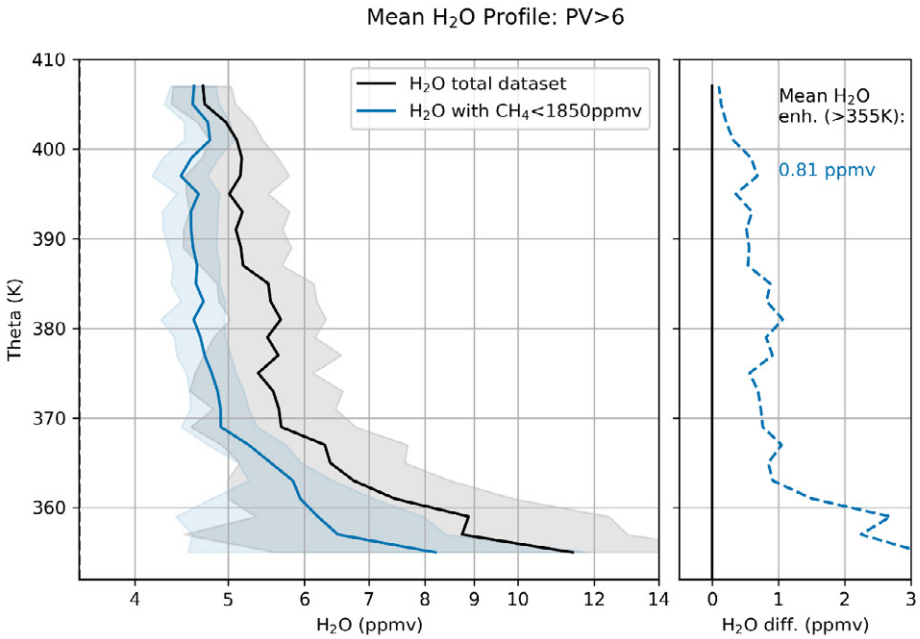

Fig. 14. (Left panel) Mean water vapor profiles as a function of potential temperature: (black line) average of all water vapor observations; (blue line) average of water vapor observations corresponding to methane values smaller than 1850 ppbv; (Right panel) Difference between the "background" profile (blue) and the mean profile. Only data points with PV greater than 6 PVU are included.

6. Summary and Discussion

During PHILEAS we studied the Asian summer monsoon's role in linking Southeast Asia's near-surface atmosphere to the extratropical upper troposphere and lower stratosphere. The Asian summer monsoon plays a key role in transporting moisture, aerosols, and pollutants, including very-short-lived chlorinated compounds, to high-latitude regions. This impacts atmospheric chemistry including ozone depletion in this region and alters the climate-relevant atmospheric radiation budget.

The observational program was based on the HALO aircraft, which was equipped with a sophisticated payload comprising 13 instruments provided by five major research institutes and three universities (see Table 2). The scientific flights were supported by a team of approximately 70 scientists and technicians. The collaboration among the various scientific teams was highly interactive throughout the campaign. Each team was responsible for preparing their respective instruments for each flight and for ensuring near-real-time data

Accepted for publication in *Bulletin of the American Meteorological Society.* DOI 10.1175/BAMS-D-24-0232.1.

processing. These efforts were critical for providing timely input into the daily flight planning meetings of all teams. A key element enabling this coordination was the use of the shared Mission Support System (see Section 2), which facilitated real-time sharing of proposed flight plans and thus supported the definition of the final flight plans.

During Phase 1, from 5 to 20 August 2023, HALO encountered the westwardly displaced lower AMA boundary over the Eastern Mediterranean region. The measurements conducted during this period reveal clear signatures of the ATAL, e.g. enhanced concentrations of solid ammonium nitrate. During Phase 2, from 21 August to 19 September 2023, the focus shifted to addressing the observational gap in the northern hemisphere at middle and high latitudes, where mixing of monsoon-influenced airmasses into the extratropical lower stratosphere occurs. The observations allowed to study the evolution of gas-phase and particulate constituents within large-scale filaments of monsoon-influenced air, transported far away from their sources in the Asian summer monsoon region.

Our observations also show the main eastward transport pathways of air from the Asian summer monsoon into the extratropical UTLS. Quantifying these transport pathways and the associated processes is crucial due to increasing emissions of anthropogenic chlorinated very short-lived substances (VSLS), which are not regulated under the Montreal Protocol and its amendments and adjustments. Chlorinated VSLS, such as dichloromethane (CH_2Cl_2), are thus becoming increasingly important for the atmospheric chlorine and ozone budget (Hossaini et al., 2019). The observed rise in chlorinated VSLS emissions in Asia is largely attributed to the increase in CH_2Cl_2 (e.g., Engel et al., 2018; Claxton et al., 2020). Remarkably, during PHILEAS, we detected particularly high mixing ratios of CH_2Cl_2 in polluted filaments within the extratropical troposphere, along with evidence of mixing into the lower stratosphere. Given that variations in ozone levels within the extratropical lower stratosphere also significantly impact on the atmosphere's radiation budget (e.g., Riese et al., 2012), it is important that future studies quantitatively analyze this contribution and its potential future changes.

Our measurements underline that the Asian summer monsoon has a significant influence on the composition of the background in the extratropical lower stratosphere. During PHILEAS, an increase in the mean water vapor mixing ratio of 0.8 ppmv was observed. Such changes in the extratropical lower stratosphere are particularly relevant, since water vapor changes in this region play a key role for the atmosphere's radiation budget (e.g., Forster and Shine, 2002, Solomon et al., 2010, Riese et al., 2012). Banerjee et al., (2019) highlight the

Accepted for publication in *Bulletin of the American Meteorological Society.* DOI 10.1175/BAMS-D-24-0232.1.

important role of water vapor changes in the extratropical lower stratosphere for the overall stratospheric water vapor feedback. In addition, the radiation budget of the extratropical lower stratosphere is influenced by the observed long-range transport of aerosols, e.g., solid ammonium nitrate aerosol particles, also affecting cirrus cloud formation.

The PHILEAS dataset is expected to support a wide range of process-oriented studies. These include investigations into the transport and mixing of monsoon-influenced air into the extratropical upper troposphere and lower stratosphere (UTLS) (e.g., Jesswein et al., 2025, Kaumanns et al., in prep.), the identification of continental and maritime source regions contributing to the outflow from the Asian summer monsoon anticyclone (e.g., Vogel et al., in prep.), and the interannual variability of monsoon-related transport into the global atmosphere (e.g., Kachula et al., 2025). Furthermore, the data will be used in conjunction with general circulation models and chemistry–climate models to study the persistence and role of monsoon-related aerosols in the stratosphere (e.g., Köllner et al., in review) as well as the monsoon's influence on the UTLS water vapor budget and associated radiative and dynamical impacts based on previous studies (e.g., Charlesworth et al., 2023; Ploeger et al., 2024).

Accepted for publication in *Bulletin of the American Meteorological Society.* DOI 10.1175/BAMS-D-24-0232.1.

Acknowledgments.

Our sincere thanks go to the DLR-FX team for conducting the aircraft measurements and providing logistical and planning support during the campaign. We would also like to thank the enviscope team of Rolf Maser for their continuous technical support during the campaign. We would like to thank the European Center for Medium-range Weather Forecasts for providing meteorological forecast data in support of the PHILEAS flight planning. Our sincere thanks go to Mike Fromm (NRL), who supported the biomass burning related measurements during the campaign with his predictions. We acknowledge that the PHILEAS mission costs for Forschungszentrum Jülich GmbH and the Karlsruhe Institute of Technology (KIT) were funded through institutional support obtained from the Helmholtz Program-Oriented Funding Scheme (POF-IV). The mission costs for TROPOS and the university partners were covered by the German Research Foundation (DFG) as part of the HALO Priority Program (SPP 1294). Additionally, several related scientific projects received funding through this program. The scientific work was further supported by projects of the TRR 301 'TPChange' program of DFG (Project-ID 428312742). Meteorological data from the German Weather Service was used to reinitialize the ICON-ART model every 24 hours. Forschungszentrum Jülich GmbH and Karlsruhe Institute of Technology received support from the ESA CAIRTEX project (4000141036/23/NL/FF/ab). The authors would like to gratefully acknowledge the computing time for the CLaMS flight planning simulations granted on the supercomputer JUWELS at Jülich Supercomputing Centre (JSC) within the Earth System Modelling (ESM) under the project ID CLaMS-ESM. Flight planning simulations were further conducted using the HoreKa supercomputer, supported by the Ministry of Science, Research, and the Arts of Baden-Württemberg, as well as the Federal Ministry of Education and Research. Our sincere thanks go to ECMWF for providing meteorological forecast data. We would like to thank Karl-Heinz Nogai for his support in creating some of the figures. We also thank ChatGPT for assisting in language refinement and improvement.

Accepted for publication in *Bulletin of the American Meteorological Society.* DOI 10.1175/BAMS-D-24-0232.1.

Data Availability Statement.

Observational data from the HALO missions are available via the HALO database (https://halo-db.pa.op.dlr.de/). CLaMS model output, e.g., on surface-origin tracers is also available via the HALO database. The ERA5 data used here are available from the ECMWF (https://www.copernicus.eu/en). ECMWF does not accept any liability Whatsoever for any error or omission in the data, their availability, or for any loss or damage arising from their use. The CLaMS model code is accessible via https://jugit.fz-juelich.de/clams/clams. The data to reproduce the analyses of this publication are available from the corresponding author upon request.

Accepted for publication in *Bulletin of the American Meteorological Society.* DOI 10.1175/BAMS-D-24-0232.1.

REFERENCES

An, M., and Coauthors, 2021: Rapid increase in dichloromethane emissions from China inferred through atmospheric observations. *Nat Commun* **12**, 7279, https://doi.org/10.1038/s41467-021-27592-y

Adcock, K. E., and Coauthors, 2021: Aircraft-based observations of ozone-depleting substances in the upper troposphere and lower stratosphere in and above the Asian summer monsoon. *J. Geophys. Res. Atmos.*, 126, e2020JD033137, https://doi.org/10.1029/2020JD033137

Appel, O., and Coauthors, 2022: Chemical analysis of the Asian tropopause aerosol layer (ATAL) with emphasis on secondary aerosol particles using aircraft-based in situ aerosol mass spectrometry, *Atmos. Chem. Phys.*, 22, 13607–13630, https://doi.org/10.5194/acp-22-13607-2022

Bakels, L., and Coauthors, 2024: FLEXPART version 11: improved accuracy, efficiency, and flexibility, *Geosci. Model Dev.*, 17, 7595–7627, https://doi.org/10.5194/gmd-17-7595-2024

Banerjee, A., and Coauthors, 2019: Stratospheric water vapor: an important climate feedback, *Clim Dyn* **53**, 1697–1710, https://doi.org/10.1007/s00382-019-04721-4

Bauer, R., Grooß, J.-U., Ungermann, J., Bär, M., Geldenhuys, M., and Hoffmann, L, 2022: The Mission Support System (MSS v7.0.4) and its use in planning for the SouthTRAC aircraft campaign, *Geosci. Model Dev.*, 15, 8983–8997, https://doi.org/10.5194/gmd-15-8983-2022

Brabec, M., Wienhold, F. G., Luo, B. P., Vömel, H., Immler, F., Steiner, P., Hausammann, E., Weers, U., and Peter, T., 2012: Particle backscatter and relative humidity measured across cirrus clouds and comparison with microphysical cirrus modelling, *Atmos. Chem. Phys.*, 12, 9135–9148, https://doi.org/10.5194/acp-12-9135-2012

Brunamonti, S., and Coauthors, 2018 Balloon-borne measurements of temperature, water vapor, ozone and aerosol backscatter on the southern slopes of the Himalayas during StratoClim 2016–2017, *Atmos. Chem. Phys.*, 18, 15937–15957, https://doi.org/10.5194/acp-18-15937-2018

Charlesworth, E., and Coauthors, 2023: Stratospheric water vapor affecting atmospheric circulation. *Nat Commun* **14**, 3925, https://doi.org/10.1038/s41467-023-39559-2

Accepted for publication in *Bulletin of the American Meteorological Society.* DOI 10.1175/BAMS-D-24-0232.1.

Claxton, T., and Coauthors, 2020: A synthesis inversion to constrain global emissions of two very short lived chlorocarbons: dichloromethane, and perchloroethylene. *J. Geophys. Res. Atmos.*, 125, https://doi.org/10.1029/2019JD031818

Clemens, J., Ploeger, F., Konopka, P., Portmann, R., Sprenger, M., and Wernli, H., 2022: Characterization of transport from the Asian summer monsoon anticyclone into the UTLS via shedding of low potential vorticity cutoffs, *Atmos. Chem. Phys.*, 22, 3841–3860, https://doi.org/10.5194/acp-22-3841-2022

Clemens, J., Vogel, B., Hoffmann, L., Griessbach, S., Thomas, N., Fadnavis, S., Müller, R., Peter, T., and Ploeger, F., 2024: A multi-scenario Lagrangian trajectory analysis to identify source regions of the Asian tropopause aerosol layer on the Indian sub-continent in August 2016, *Atmos. Chem. Phys.*, 24, 763–787, https://doi.org/10.5194/acp-24-763-2024

Curtius, J., and Coauthors, 2024: Isoprene nitrates drive new particle formation in Amazon's upper troposphere. *Nature,* 636, 124–130, https://doi.org/10.1038/s41586-024-08192-4

Dethof, A., A. O'Neill, J.M. Slingo, and H.G.J. Smit, 1999: A mechanism for moistening the lower stratosphere involving the Asian summer monsoon, Q. J. R. Meteorol. Soc., 125, 1079–1106, https://doi.org/10.1002/qj.1999.49712555602

Dragoneas, A., Molleker, S., Appel, O., Hünig, A., Böttger, T., Hermann, M., Drewnick, F., Schneider, J., Weigel, R., and Borrmann, S., 2022: The realization of autonomous, aircraft-based, real-time aerosol mass spectrometry in the upper troposphere and lower stratosphere, *Atmos. Meas. Tech.*, 15, 5719–5742, https://doi.org/10.5194/amt-15-5719-2022

Engel, A., and Coauthors, 2018: Update on ozone-depleting substances (ODSs) and other gases of interest to the Montreal Protocol, *Scientific Assessment of Ozone Depletion: 2018,* Global Ozone Research and Monitoring Project-Rep. No. 58, World Meteorological Organization, Geneva, Switzerland.

Fadnavis, S., Semeniuk, K., Pozzoli, L., Schultz, M. G., Ghude, S. D., Das, S., and Kakatkar, R., 2013: Transport of aerosols into the UTLS and their impact on the Asian monsoon region as seen in a global model simulation, *Atmos. Chem. Phys.*, 13, 8771–8786, https://doi.org/10.5194/acp-13-8771-2013

Accepted for publication in *Bulletin of the American Meteorological Society.* DOI 10.1175/BAMS-D-24-0232.1.

Fadnavis, S., Sagalgile, A., Sonbawne, S., Vogel, B., Peter, Th., Wienhold, F. G., Dirksen, R., Oelsner, P. and Müller, R., 2023: Comparison of ozone sonde measurements in the upper troposphere and lower Stratosphere in Northern India with reanalysis and chemistry-climate-model data, *Sci. Rep.*, 13, 7133, https://doi.org/10.1038/s41598-023-34330-5

Forster, P. M. de F., and Shine, K. P., 2002: Assessing the climate impact of trends in stratospheric water vapor, *Geophys. Res. Lett.*, 29(6), https://doi.org/10.1029/2001GL013909

Friedl-Vallon, F., and Coauthors, 2014: Instrument concept of the imaging Fourier transform spectrometer GLORIA, *Atmos. Meas. Tech.*, 7, 3565–3577, https://doi.org/10.5194/amt-7-3565-2014

Garny, H., and Randel, W. J., 2013: Dynamic variability of the Asian monsoon anticyclone observed in potential vorticity and correlations with tracer distributions, *J. Geophys. Res. Atmos.*, 118, 13,421–13,433, https://doi.org/10.1002/2013JD020908

Gettelman, A., Hoor, P., Pan, L. L., Randel, W. J., Hegglin, M. I. and Birner, T., 2011: The extratropical upper troposphere and lower stratosphere, *Rev. Geophys.*, 49, RG3003, https://doi.org/10.1029/2011RG000355

Gill, A. E.: Some simple solutions for heat-induced tropical circulation, 1980: Q. J. R. Meteorol. Soc., 106, 447–462.

Hanumanthu, S., and Coauthors, 2020: Strong day-to-day variability of the Asian Tropopause Aerosol Layer (ATAL) in August 2016 at the Himalayan foothills, *Atmos. Chem. Phys.*, 20, 14273-14302, https://doi.org/10.5194/acp-20-14273-2020

Hersbach H., and Coauthors, 2020: The ERA5 global reanalysis. *QJ Roy Meteorol Soc*, 2020; 146: 1999–2049. https://doi.org/10.1002/qj.3803

Höpfner, M., and Coauthors, 2019: Ammonium nitrate particles formed in upper troposphere from ground ammonia sources during Asian monsoons, *Nature Geoscience*, 12 (8), pp. 608-612, https://doi.org/10.1038/s41561-019-0385-8

Hossaini, R., and Coauthors, 2019: Recent trends in stratospheric chlorine from very short-lived substances. *J. Geophys. Res. Atmos.*, 124, 2318–2335. https://doi.org/10.1029/2018JD029400

Hünig, A., and Coauthors, 2022: Design, characterization, and first field deployment of a novel aircraft-based aerosol mass spectrometer combining the laser ablation and flash

Accepted for publication in *Bulletin of the American Meteorological Society.* DOI 10.1175/BAMS-D-24-0232.1.

vaporization techniques, *Atmos. Meas. Tech.*, 15, 2889–2921, https://doi.org/10.5194/amt-15-2889-2022

Hsu, C. J., and Plumb, R. A., 2000: Nonaxisymmetric thermally driven circulations and upper-tropospheric monsoon dynamic. *J. Atmos. Sci.*, 57, 1255–1276

Jesswein, and Coauthors, 2025: Tracing elevated abundance of CH_2Cl_2 in the subarctic upper troposphere to the Asian Summer Monsoon, EGUsphere [preprint], https://doi.org/10.5194/egusphere-2024-3946.

Johansson, S., and Coauthors, 2024: Ammonia in the upper troposphere–lower stratosphere (UTLS): GLORIA airborne measurements for CAMS model evaluation in the Asian monsoon and in biomass burning plumes above the South Atlantic, *Atmos. Chem. Phys.*, 24, 8125–8138, https://doi.org/10.5194/acp-24-8125-2024

Jurkat, T., Kaufmann, S., Voigt, C., Schäuble, D., Jeßberger, P., and Ziereis, H., 2016: The airborne mass spectrometer AIMS – Part 2: Measurements of trace gases with stratospheric or tropospheric origin in the UTLS, *Atmos. Meas. Tech.*, 9, 1907–1923, https://doi.org/10.5194/amt-9-1907-2016

Kachula, O., Vogel, B., Günther, G., and Müller, R., 2025: Interannual variability of the Asian summer monsoon anticyclone, EGUsphere [preprint], https://doi.org/10.5194/egusphere-2025-1670

Kaufmann, M., and Coauthors, 2015: Retrieval of three-dimensional small-scale structures in upper-tropospheric/lower-stratospheric composition as measured by GLORIA, *Atmos. Meas. Tech.*, 8, 81–95, https://doi.org/10.5194/amt-8-81-2015

Keber, T., and Coauthors, 2020: Bromine from short-lived source gases in the extratropical northern hemispheric upper troposphere and lower stratosphere (UTLS), *Atmos. Chem. Phys.*, 20, 4105–4132, https://doi.org/10.5194/acp-20-4105-2020

Kloss, C., and Coauthors, 2021: Airborne Mid-Infrared Cavity enhanced Absorption spectrometer (AMICA), Atmos. Meas. Tech., 14, 5271–5297, https://doi.org/10.5194/amt-14-5271-2021

Krasauskas, L., and Coauthors, 2021: 3-D tomographic observations of Rossby wave breaking over the North Atlantic during the WISE aircraft campaign in 2017, *Atmos. Chem. Phys.*, 21, 10249–10272, https://doi.org/10.5194/acp-21-10249-2021

Accepted for publication in *Bulletin of the American Meteorological Society.* DOI 10.1175/BAMS-D-24-0232.1.

Krautstrunk, M. and A. Giez, 2012: The Transition from FALCON to HALO Era Airborne Atmospheric Research. In: Schumann, U. (eds) *Atmospheric Physics*. Research Topics in Aerospace. Springer, Berlin, Heidelberg,https://doi.org/10.1007/978-3-642-30183-4_37

Kremser, S., and Coauthors, 2016; Stratospheric aerosol—Observations, processes, and impact on climate, *Rev. Geophys.*, 54, 278–335, https://doi.org/10.1002/2015RG000511

Kunkel, D., Hoor, P., Kaluza, T., Ungermann, J., Kluschat, B., Giez, A., Lachnitt, H.-C., Kaufmann, M., and Riese, M., 2019: Evidence of small-scale quasi-isentropic mixing in ridges of extratropical baroclinic waves, *Atmos. Chem. Phys.*, 19, 12607–12630, https://doi.org/10.5194/acp-19-12607-2019

Kunz, A., Konopka P., Müller, R. and Pan, L., 2011: The dynamical tropopause based on isentropic potential vorticity gradients *J. Geophys. Res.*, 116, D01110, https://doi.org/10.1029/2010JD014343

Lacis, A. A., Wuebbles, D. J., and Logan, J. A., 1990: Radiative forcing of climate by changes in the vertical distribution of ozone, *J. Geophys. Res.*, 95(D7), 9971–9981, https://doi.org/10.1029/JD095iD07p09971

Lau, W. K., Yuan, C., and Li, Z., 2018: Origin, maintenance and variability of the Asian Tropopause Aerosol Layer (ATAL): the roles of monsoon dynamics, *Sci. Rep.*, 8, 3960, https://doi.org/10.1038/s41598-018-22267-z

Lauther, V., Vogel, B., Wintel, J., Rau, A., Hoor, P., Bense, V., Müller, R., and Volk, C. M., 2022: In situ observations of CH_2Cl_2 and $CHCl_3$ show efficient transport pathways for very short-lived species into the lower stratosphere via the Asian and the North American summer monsoon, *Atmos. Chem. Phys.*, 22, 2049–2077, https://doi.org/10.5194/acp-22-2049-2022

Lelieveld, J. and Coauthors, 2018: The South Asian monsoon—pollution pump and purifier, *Science,* 361, 270-273, https://doi.org/10.1126/science.aar2501

Lucke, J., and Coauthors, 2023, Characterization of Atmospheric Icing Conditions during the HALO-$(AC)^3$ Campaign with the Nevzorov Probe and the Backscatter Cloud Probe with Polarization Detection, *SAE Technical Paper* 2023-01-1485, https://doi.org/10.4271/2023-01-1485

Mahnke, C., and Coauthors, 2021: The Asian tropopause aerosol layer within the 2017 monsoon anticyclone: microphysical properties derived from aircraft-borne in situ

Accepted for publication in *Bulletin of the American Meteorological Society.* DOI 10.1175/BAMS-D-24-0232.1.

measurements, Atmos. Chem. Phys., 21, 15259–15282, https://doi.org/10.5194/acp-21-15259-2021

Marsing, A., Jurkat-Witschas, T., Grooß, J.-U., Kaufmann, S., Heller, R., Engel, A., Hoor, P., Krause, J., and Voigt, C., 2019: Chlorine partitioning in the lowermost Arctic vortex during the cold winter 2015/2016, *Atmos. Chem. Phys.*, 19, 10757–10772, https://doi.org/10.5194/acp-19-10757-2019

Meyer, J., and Coauthors, 2015: Two decades of water vapor measurements with the FISH fluorescence hygrometer: a review, *Atmos. Chem. Phys.*, 15, 8521–8538, https://doi.org/10.5194/acp-15-8521-2015

Moser, M., and Coauthors, 2023: Microphysical and thermodynamic phase analyses of Arctic low-level clouds measured above the sea ice and the open ocean in spring and summer, *Atmos. Chem. Phys.*, 23, 7257–7280, https://doi.org/10.5194/acp-23-7257-2023

Müller, S., Hoor, P., Berkes, F., Bozem, H., Klingebiel, M., Reutter, P., Smit, H. G. J., Wendisch, M., Spichtinger, P. and Borrmann, S., 2015: In situ detection of stratosphere-troposphere exchange of cirrus particles in the midlatitudes. *Geophys. Res. Lett.*, 42: 949–955, https://doi.org/10.1002/2014GL062556.

Müller, S., and Coauthors, 2016: Impact of the Asian monsoon on the extratropical lower stratosphere: trace gas observations during TACTS over Europe 2012, *Atmos. Chem. Phys.*, 16, 10573–10589, https://doi.org/10.5194/acp-16-10573-2016

Oelhaf, H., and Coauthors, 2019: POLSTRACC: Airborne Experiment for Studying the Polar Stratosphere in a Changing Climate with the High Altitude and Long Range Research Aircraft (HALO), *Bull. Amer. Meteor. Soc.*, 100(12), 2634-2664, https://doi.org/10.1175/BAMS-D-18-0181.1

Pan, L. L., Honomichl, S. B., Kinnison, D. E., Abalos, M., Randel, W. J., Bergman, J. W., and Bian, J., 2016: Transport of chemical tracers from the boundary layer to stratosphere associated with the dynamics of the Asian summer monsoon, *J. Geophys. Res. Atmos.*, 121, 14,159–14,174, https://doi.org/10.1002/2016JD025616

Pan, L.L., and coauthors, 2024: East Asian summer monsoon delivers large abundances of very-short-lived organic chlorine substances to the lower stratosphere, *Proceedings of the National Academy of Sciences of the United States of America*, 121(12), e2318716121, https://doi.org/10.1073/pnas.2318716121

Accepted for publication in *Bulletin of the American Meteorological Society.* DOI 10.1175/BAMS-D-24-0232.1.

Park, M., Randel, W. J., Gettelman, A., Massie, S. T. and Jiang, J. H., 2007: Transport above the Asian summer monsoon anticyclone inferred from Aura Microwave Limb Sounder tracers, *J. Geophys. Res.*, 112, D16309, doi:10.1029/2006JD008294.

Park, M., Randel, W. J., Emmons, L. K., Bernath, P. F., Walker, K. A., and Boone, C. D., 2008: Chemical isolation in the Asian monsoon anticyclone observed in Atmospheric Chemistry Experiment (ACE-FTS) data, *Atmos. Chem. Phys.*, 8, 757–764, https://doi.org/10.5194/acp-8-757-2008

Ploeger, F., G. Günther, P. Konopka, S. Fueglistaler, R. Müller, C. Hoppe, A. Kunz, R. Spang, J.-U. Grooß, and M. Riese, 2013: Horizontal water vapor transport in the lower stratosphere from subtropics to high latitudes during boreal summer, *J. Geophys. Res. Atmos.*, 118, 8111–8127, https://doi.org/10.1002/jgrd.50636

Ploeger, F., Gottschling, C., Griessbach, S., Grooß, J.-U., Guenther, G., Konopka, P., Müller, R., Riese, M., Stroh, F., Tao, M., Ungermann, J., Vogel, B., and von Hobe, M., 2015: A potential vorticity-based determination of the transport barrier in the Asian summer monsoon anticyclone, *Atmos. Chem. Phys.*, 15, 13145–13159, https://doi.org/10.5194/acp-15-13145-2015

Ploeger, F. and Birner, T., 2016: Seasonal and inter-annual variability of lower stratospheric age of air spectra, *Atmos. Chem. Phys.*, 16, 10195–10213, https://doi.org/10.5194/acp-16-10195-2016

Ploeger, F., Konopka, P., Walker, K., and Riese, M., 2017: Quantifying pollution transport from the Asian monsoon anticyclone into the lower stratosphere, *Atmos. Chem. Phys.*, 17, 7055–7066, https://doi.org/10.5194/acp-17-7055-2017

Ploeger, F., Diallo, M., Charlesworth, E., Konopka, P., Legras, B., Laube, J. C., Grooß, J.-U., Günther, G., Engel, A., and Riese, M., 2021: The stratospheric Brewer–Dobson circulation inferred from age of air in the ERA5 reanalysis, *Atmos. Chem. Phys.*, 21, 8393– 8412, https://doi.org/10.5194/acp-21-8393-2021

Ploeger, F., Birner, T., Charlesworth, E., Konopka, P., and Müller, R., 2024: Moist bias in the Pacific upper troposphere and lower stratosphere (UTLS) in climate models affects regional circulation patterns, *Atmos. Chem. Phys.*, 24, 2033–2043, https://doi.org/10.5194/acp-24-2033-2024

Accepted for publication in *Bulletin of the American Meteorological Society.* DOI 10.1175/BAMS-D-24-0232.1.

Pommrich, R., and Coauthors, 2014: Tropical troposphere to stratosphere transport of carbon monoxide and long-lived trace species in the Chemical Lagrangian Model of the Stratosphere (CLaMS), *Geosci. Model Dev.*, 7, 2895–2916, https://doi.org/10.5194/gmd-7-2895-2014

Popovic, J. M. and Plumb, R. A., 2001: Eddy Shedding from the Upper-Tropospheric Asian Monsoon Anticyclone, *J. Atmos. Sci.*, 58, 93–104, https://doi.org/10.1175/1520-0469(2001)058<0093:ESFTUT>2.0.CO;2

Popp, P. J., and Coauthors, 2007: Condensed-phase nitric acid in a tropical subvisible cirrus cloud, *Geophys. Res. Lett.,* 34, L24812, https://doi.org/10.1029/2007GL031832

Randel, W. J., Park, M., Emmons, L., Kinnison, D., Bernath, P., Walker, K. A., Boone, C., and Pumphrey, H., 2010: Asian Monsoon Transport of Pollution to the Stratosphere, *Science*, 328, 611–613, https://doi.org/10.1126/science.1182274

Randel, W. J. and Jensen, E. J., 2013: Physical Processes in the Tropical Tropopause Layer and Their Roles in a Changing Climate. *Nature Geoscience*, 6, 169-176. https://doi.org/10.1038/ngeo1733

Rautenhaus, M., G., Bauer, R., and Dörnbrack, A., 2012: A web service based tool to plan atmospheric research flights, *Geosci. Model Dev.*, 5, 55–71, https://doi.org/10.5194/gmd-5-55-2012

Riehl, H., 1954: Tropical Meteorology, McGraw-Hill Publishing Company LTD, New York, London, Toronto.

Riese, M., Ploeger, F., Rap, A., Vogel, B., Konopka, P., Dameris, M., and Forster, P., 2012: Impact of uncertainties in atmospheric mixing on simulated UTLS composition and related radiative effects, *J. Geophys. Res.*, 117, D16305, https://doi.org/10.1029/2012JD017751

Riese, M., and Coauthors, 2014: Gimballed Limb Observer for Radiance Imaging of the Atmosphere (GLORIA) scientific objectives, *Atmos. Meas. Tech.*, 7, 1915–1928, https://doi.org/10.5194/amt-7-1915-2014

Rolf, C., Vogel, B., Hoor, P., Afchine, A., Günther, G., Krämer, M., Müller, R., Müller, S., Spelten, N., and Riese, M., 2018: Water vapor increase in the lower stratosphere of the Northern Hemisphere due to the Asian monsoon anticyclone observed during the TACTS/ESMVal campaigns, *Atmos. Chem. Phys.*, 18, 2973–2983,

Accepted for publication in *Bulletin of the American Meteorological Society.* DOI 10.1175/BAMS-D-24-0232.1.

https://doi.org/10.5194/acp-18-2973-2018

Santee, M. L., G. L. Manney, N. J. Livesey, M. J. Schwartz, J. L. Neu, and W. G. Read, 2017: A comprehensive overview of the climatological composition of the Asian summer monsoon anticyclone based on 10 years of Aura Microwave Limb Sounder measurements, *J. Geophys. Res. Atmos.*, 122, 5491–5514, https://doi.org/10.1002/2016JD026408

Singh, H. B., and Coauthors, 2007: Reactive nitrogen distribution and partitioning in the North American troposphere and lowermost stratosphere, *J. Geophys. Res.*, 112, D12S04, https://doi.org/10.1029/2006JD007664

Schröter, J., and Coauthors, 2018: ICON-ART 2.1: a flexible tracer framework and its application for composition studies in numerical weather forecasting and climate simulations, *Geosci. Model Dev.*, 11, 4043–4068, https://doi.org/10.5194/gmd-11-4043-2018

Siu, W.S., and K.W., Bowmann, 2020: Unsteady Vortex Behavior in the Asian Monsoon Anticyclone, *J. Atmos. Sci.*, 77, 12, 4067-4088, https://doi.org/10.1175/JAS-D-19-0349.1Solomon, S., Rosenlof, K. H., Portman, R. W., Daniel, J. S., Davis, S. M.T, Sanford, T. J., and Plattner, G.-K. 2010: Contributions of stratospheric water vapor to decadal changes in the rate of global warming, *Science*, 327, 1219–1223, https://doi.og/10.1126/science.1182488

Tomsche, L., Pozzer, A., Ojha, N., Parchatka, U., Lelieveld, J., and Fischer, H., 2019: Upper tropospheric CH_4 and CO affected by the South Asian summer monsoon during the Oxidation Mechanism Observations mission, Atmos. Chem. Phys., 19, 1915–1939, https://doi.org/10.5194/acp-19-1915-2019

Tomsche, L., and Co-Authors, 2022: Enhanced sulfur in the upper troposphere and lower stratosphere in spring 2020, *Atmos. Chem. Phys.*, 22, 15135–15151, https://doi.org/10.5194/acp-22-15135-2022

Turhal, K., Plöger, F., Clemens, J., Birner, T., Weyland, F., Konopka, P., and Hoor, P., 2024: Variability and trends in the PV-gradient dynamical tropopause, *EGUsphere* [preprint], https://doi.org/10.5194/egusphere-2024-471

Ungermann, J., Blank, J., Lotz, J., Leppkes, K., Hoffmann, L., Guggenmoser, T., Kaufmann, M., Preusse, P., Naumann, U., and Riese, M., 2011: A 3-D tomographic retrieval approach with advection compensation for the air-borne limb-imager GLORIA, *Atmos. Meas. Tech.*, 4, 2509–2529, https://doi.org/10.5194/amt-4-2509-2011

Accepted for publication in *Bulletin of the American Meteorological Society.* DOI 10.1175/BAMS-D-24-0232.1.

Ungermann, J., Ern, M., Kaufmann, M., Müller, R., Spang, R., Ploeger, F., Vogel, B., and Riese, M., 2016: Observations of PAN and its confinement in the Asian summer monsoon anticyclone in high spatial resolution, *Atmos. Chem. Phys.*, 16, 8389–8403, https://doi.org/10.5194/acp-16-8389-2016

Vömel, H., Naebert, T., Dirksen, R., and Sommer, M., 2016: An update on the uncertainties of water vapor measurements using cryogenic frost point hygrometers, *Atmos. Meas. Tech.*, 9, 3755–3768, https://doi.org/10.5194/amt-9-3755-2016

Vogel, B., Günther, G., Müller, R., Grooß, J.-U., Hoor, P., Krämer, M., Müller, S., Zahn, A., and Riese, M., 2014: Fast transport from Southeast Asia boundary layer sources to northern Europe: rapid uplift in typhoons and eastward eddy shedding of the Asian monsoon anticyclone, *Atmos. Chem. Phys.*, 14, 12745–12762, https://doi.org/10.5194/acp-14-12745-2014

Vogel, B., Günther, G., Müller, R., Grooß, J.-U., and Riese, M., 2015: Impact of different Asian source regions on the composition of the Asian monsoon anticyclone and of the extratropical lowermost stratosphere, *Atmos. Chem. Phys.*, 15, 13699–13716, https://doi.org/10.5194/acp-15-13699-2015

Vogel, B., and Coauthors, 2016: Long-range transport pathways of tropospheric source gases originating in Asia into the northern lower stratosphere during the Asian monsoon season 2012, *Atmos. Chem. Phys.*, 16, 15301–15325, https://doi.org/10.5194/acp-16-15301-2016

Vogel, B., Müller, R., Günther, G., Spang, R., Hanumanthu, S., Li, D., Riese, M., and Stiller, G. P., 2019: Lagrangian simulations of the transport of young air masses to the top of the Asian monsoon anticyclone and into the tropical pipe, *Atmos. Chem. Phys.*, 19, 6007–6034, https://doi.org/10.5194/acp-19-6007-2019

Vogel, B., Volk, C. M., Wintel, J., Lauther, V., Müller, R., Patra, P. K., Riese, M., Terao, Y., and Stroh, F., 2023: Reconstructing high-resolution in-situ vertical carbon dioxide profiles in the sparsely monitored Asian monsoon region, *Comm Earth Environ*, 4, https://doi.org/10.1038/s43247-023-00725-5

Voigt, C., and Coauthors, 2017: ML-CIRRUS - The airborne experiment on natural cirrus and contrail cirrus with the high-altitude long-range research aircraft HALO, *Bull. Amer. Meteor. Soc.*, https://doi.org/10.1175/BAMS-D-15-00213.1

Accepted for publication in *Bulletin of the American Meteorological Society.* DOI 10.1175/BAMS-D-24-0232.1.

von Hobe, M., and Coauthors, 2021: Upward transport into and within the Asian monsoon anticyclone as inferred from StratoClim trace gas observations, *Atmos. Chem. Phys.*, 21, 1267–1285, https://doi.org/10.5194/acp-21-1267-2021

Wagner, R., Bertozzi, B., Höpfner, M., Höhler, K., Möhler, O., Saathoff, H., & Leisner, T., 2020: Solid ammonium nitrate aerosols as efficient ice nucleating particles at cirrus temperatures, *J. Geophys. Res. Atmos.*, 125, e2019JD032248. https://doi.org/10.1029/2019JD032248

Waters, J.W., and Coauthors, 2006: The Earth Observing System Microwave Limb Sounder (EOS MLS) on the Aura satellite, *IEEE Trans. Geosci. Remote Sensing 44*, no. 5, https://doi.org/10.1109/TGRS.2006.873771

Weigel, R., and Coauthors, 2021: In situ observation of new particle formation (NPF) in the tropical tropopause layer of the 2017 Asian monsoon anticyclone – Part 1: Summary of StratoClim results, Atmos. Chem. Phys., 21, 11689–11722, https://doi.org/10.5194/acp-21-11689-2021Weimer, M., and Coauthors, 2017: An emission module for ICON-ART 2.0: implementation and simulations of acetone, *Geosci. Model Dev.*, 10, 2471–2494, https://doi.org/10.5194/gmd-10-2471-2017

Wetzel, G., and Coauthors, 2021: Pollution trace gases C2H6, C2H2, HCOOH, and PAN in the North Atlantic UTLS: observations and simulations, *Atmos. Chem. Phys.*, 21, 8213–8232, https://doi.org/10.5194/acp-21-8213-2021

Xenofontos, C., and Coauthors, 2024: The impact of ammonia on particle formation in the Asian Tropopause Aerosol Layer. *npj Clim Atmos Sci* **7**, 215, https://doi.org/10.1038/s41612-024-00758-3

Yan, X., Konopka, P., Ploeger, F., Podglajen, A., Wright, J. S., Müller, R., and Riese, M., 2019: The efficiency of transport into the stratosphere via the Asian and North American summer monsoon circulations, Atmos. Chem. Phys., 19, 15629–15649, https://doi.org/10.5194/acp-19-5629-2019

Zahn, A., Weppner, J., Widmann, H., Schlote-Holubek, K., Burger, B., Kühner, T., and Franke, H., 2012: A fast and precise chemiluminescence ozone detector for eddy flux and airborne application, *Atmos. Meas. Tech.*, 5, 363–375, https://doi.org/10.5194/amt-5-363-2012

Accepted for publication in *Bulletin of the American Meteorological Society.* DOI 10.1175/BAMS-D-24-0232.1.

Zängl, G., Reinert, D., Ripodas, P., and Baldauf, M., 2015: The ICON (ICOsahedral Non-hydrostatic) modelling framework of DWD and MPI-M: Description of the non-hydrostatic dynamical core, *QJ Roy Meteorol Soc.*, 141, 563–579, https://doi.org/10.1002/qj.2378

Ziereis, H., and Coauthors, 2022: Redistribution of total reactive nitrogen in the lowermost Arctic stratosphere during the cold winter 2015/2016, *Atmos. Chem. Phys.*, 22, 3631-3654, https://doi.org/10.5194/acp-22-3631-2022

Zöger, M., and Coauthors, 1999: Fast in situ stratospheric hygrometers: A new family of balloon-borne and airborne Lyman α photofragment fluorescence hygrometers, *J. Geophys. Res.*, 104 (D1), 1807–1816, https://doi.org/10.1029/1998JD100024

Accepted for publication in *Bulletin of the American Meteorological Society.* DOI 10.1175/BAMS-D-24-0232.1.